nature genetics

Plasmodium cynomolgi genome sequences provide insight into *Plasmodium vivax* and the monkey malaria clade

Shin-Ichiro Tachibana[1,13], Steven A Sullivan[2], Satoru Kawai[3], Shota Nakamura[4], Hyunjae R Kim[2], Naohisa Goto[4], Nobuko Arisue[5], Nirianne M Q Palacpac[5], Hajime Honma[1,5], Masanori Yagi[5], Takahiro Tougan[5], Yuko Katakai[6], Osamu Kaneko[7], Toshihiro Mita[8], Kiyoshi Kita[9], Yasuhiro Yasutomi[10], Patrick L Sutton[2], Rimma Shakhbatyan[2], Toshihiro Horii[5], Teruo Yasunaga[4], John W Barnwell[11], Ananias A Escalante[12], Jane M Carlton[2,14] & Kazuyuki Tanabe[1,5,14]

***P. cynomolgi*, a malaria-causing parasite of Asian Old World monkeys, is the sister taxon of *P. vivax*, the most prevalent malaria-causing species in humans outside of Africa. Because *P. cynomolgi* shares many phenotypic, biological and genetic characteristics with *P. vivax*, we generated draft genome sequences for three *P. cynomolgi* strains and performed genomic analysis comparing them with the *P. vivax* genome, as well as with the genome of a third previously sequenced simian parasite, *Plasmodium knowlesi*. Here, we show that genomes of the monkey malaria clade can be characterized by copy-number variants (CNVs) in multigene families involved in evasion of the human immune system and invasion of host erythrocytes. We identify genome-wide SNPs, microsatellites and CNVs in the *P. cynomolgi* genome, providing a map of genetic variation that can be used to map parasite traits and study parasite populations. The sequencing of the *P. cynomolgi* genome is a critical step in developing a model system for *P. vivax* research and in counteracting the neglect of *P. vivax*.**

Human malaria is transmitted by anopheline mosquitoes and is caused by four species in the genus *Plasmodium*. Of these, *P. vivax* is the major malaria agent outside of Africa, annually causing 80–100 million cases[1]. Although *P. vivax* infection is often mistakenly regarded as benign and self-limiting, *P. vivax* treatment and control present challenges distinct from those of the more virulent *Plasmodium falciparum*. Biological traits, including a dormant (hypnozoite) liver stage responsible for recurrent infections (relapses), early infective sexual stages (gametocytes) and transmission from low parasite densities in the blood[2], coupled with emerging antimalarial drug resistance[3], render *P. vivax* resilient to modern control strategies. Recent evidence indicates that *P. falciparum* derives from parasites of great apes in Africa[4], whereas *P. vivax* is more closely related to parasites of Asian Old World monkeys[5–7], although not itself infective of these monkeys.

P. vivax cannot be cultured *in vitro*, and the small New World monkeys capable of hosting it are rare and do not provide an ideal model system. *P. knowlesi*, an Asian Old World monkey parasite recently recognized as a zoonosis for humans[8], has had its genome sequenced[9], but the species is distantly related to *P. vivax* and is phenotypically dissimilar. In contrast, *P. cynomolgi*, a simian parasite that can infect humans experimentally[10], is the closest living relative (a sister taxon) to *P. vivax* and possesses most of the same genetic, phenotypic and biological characteristics—notably, periodic relapses caused by dormant hypnozoites, early infectious gametocyte formation and invasion of Duffy blood group–positive reticulocytes. *P. cynomolgi* thus offers a robust model for *P. vivax* in a readily available laboratory host, the Rhesus monkey, whose genome was recently sequenced[11]. Here, we report draft genome sequences of three *P. cynomolgi* strains and comparative genomic analyses of *P. cynomolgi*, *P. vivax*[12] and *P. knowlesi*[9], three members of the monkey malaria clade.

We sequenced the genome of *P. cynomolgi* strain B, isolated from a monkey in Malaysia and grown in splenectomized monkeys (Online Methods). A combination of Sanger, Roche 454 and Illumina chemistries was employed to generate a high-quality reference assembly at 161-fold coverage, consisting of 14 supercontigs (corresponding to the 14 parasite chromosomes) and ~1,649 unassigned contigs, comprising

[1]Laboratory of Malariology, Research Institute for Microbial Diseases, Osaka University, Suita, Japan. [2]Department of Biology, Center for Genomics and Systems Biology, New York University, New York, New York, USA. [3]Laboratory of Tropical Medicine and Parasitology, Institute of International Education and Research, Dokkyo Medical University, Shimotsuga, Japan. [4]Genome Information Research Center, Research Institute for Microbial Diseases, Osaka University, Suita, Japan. [5]Department of Molecular Protozoology, Research Institute for Microbial Diseases, Osaka University, Suita, Japan. [6]The Corporation for Production and Research of Laboratory Primates, Tsukuba, Japan. [7]Department of Protozoology, Institute of Tropical Medicine (NEKKEN) and Global COE (Centers of Excellence) Program, Nagasaki University, Nagasaki, Japan. [8]Department of Molecular and Cellular Parasitology, Graduate School of Medicine, Juntendo University, Tokyo, Japan. [9]Department of Biomedical Chemistry, Graduate School of Medicine, The University of Tokyo, Tokyo, Japan. [10]Tsukuba Primate Research Center, National Institute of Biomedical Innovation, Tsukuba, Japan. [11]Center for Global Health, Centers for Disease Control and Prevention, Divison of Parasitic Diseases and Malaria, Atlanta, Georgia, USA. [12]Center for Evolutionary Medicine and Informatics, The Biodesign Institute, Arizona State University, Tempe, Arizona, USA. [13]Present address: Career-Path Promotion Unit for Young Life Scientists, Kyoto University, Kyoto, Japan. [14]These authors jointly directed this work. Correspondence should be addressed to K.T. (kztanabe@biken.osaka-u.ac.jp) or J.M.C. (jane.carlton@nyu.edu).

Received 25 January; accepted 9 July; published online 5 August 2012; doi:10.1038/ng.2375

a total length of ~26.2 Mb (**Supplementary Table 1**). Comparing genomic features of *P. cynomolgi*, *P. knowlesi* and *P. vivax* reveals many similarities, including GC content (mean GC content of 40.5%), 14 positionally conserved centromeres and the presence of intrachromosomal telomeric sequences (ITSs; GGGTT(T/C)A), which were discovered in the *P. knowlesi* genome[9] but are absent in *P. vivax* (**Fig. 1**, **Table 1** and **Supplementary Table 2**).

We annotated the *P. cynomolgi* strain B genome using a combination of *ab initio* gene prediction programs trained on high-quality data sets and sequence similarity searches against the annotated *P. vivax* and *P. knowlesi* genomes. Not unexpectedly for species from the same monkey malaria clade, gene synteny along the 14 chromosomes is highly conserved, although numerous microsyntenic breaks are present in regions containing multigene families (**Fig. 2** and **Table 2**). This genome-wide view of synteny in six species of *Plasmodium* also identified two apparent errors in existing public sequence databases: an inversion in chromosome 3 of *P. knowlesi* and an inversion in chromosome 6 of *P. vivax*. The *P. cynomolgi* genome contains 5,722 genes, of which approximately half encode conserved hypothetical proteins of unknown function, as is the case in all the *Plasmodium* genomes sequenced to date. A maximum-likelihood phylogenetic tree constructed using 192 conserved ribosomal and translation- and transcription-related genes (**Supplementary Fig. 1**) confirms the close relationship of *P. cynomolgi* to *P. vivax* compared to five other *Plasmodium* species. Approximately 90% of genes (4,613) have reciprocal best-match orthologs in all three species (**Fig. 3**), enabling refinement of the existing *P. vivax* and *P. knowlesi* annotations (**Supplementary Table 3**). The high degree of gene orthology enabled us to identify specific examples of gene duplication (an important vehicle for genome evolution), including a duplicated homolog of *P. vivax Pvs28*—which encodes a sexual stage surface antigen that is a transmission-blocking vaccine candidate[13]—in *P. cynomolgi* (**Supplementary Table 4**). Genes common only to *P. cynomolgi* and *P. vivax* (n = 214) outnumber those that are restricted to *P. cynomolgi* and *P. knowlesi* (n = 100) or *P. vivax* and *P. knowlesi* (n = 17). Such figures establish the usefulness of *P. cynomolgi* as a model species for studying the more intractable *P. vivax*.

Notably, most of the genes specific to a particular species belong to multigene families (excluding hypothetical genes; **Table 2** and **Supplementary Table 5**). This suggests repeated lineage-specific gene duplication and/or gene deletion in multigene families within the three monkey malaria clade species. Moreover, copy numbers of the genes composing multigene families were generally greater in the *P. cynomolgi–P. vivax* lineage than in *P. knowlesi*, suggesting repeated gene duplication in the ancestral lineage of *P. cynomolgi* and *P. vivax* (or repeated gene deletion in the *P. knowlesi* lineage). Thus, the genomes of *P. cynomolgi*, *P. vivax* and *P. knowlesi* can largely be distinguished by variations in the copy number of multigene family members. Examples of such families include those that encode proteins involved in evasion of the human immune system (*vir*, *kir* and *SICAvar*) and invasion of host red blood cells (*dbp* and *rbp*).

In malaria-causing parasites, invasion of host erythrocytes, mediated by specific interactions between parasite ligands and erythrocyte receptors, is a crucial component of the parasite lifecycle. Of great interest are the *ebl* and *rbl* gene families, which encode parasite ligands required for the recognition of host erythrocytes. The *ebl* genes encode erythrocyte binding–like (EBL) ligands such as the Duffy-binding proteins (DBPs) that bind to Duffy antigen receptor for chemokines (DARC) on human and monkey erythrocytes. The *rbl* genes encode the reticulocyte binding–like (RBL) protein family, including reticulocyte-binding proteins (RBPs) in *P. cynomolgi* and *P. vivax*, and normocyte-binding proteins (NBPs) in *P. knowlesi*, which bind to unknown erythrocyte receptors[14]. We confirmed the presence of two *dbp* genes in *P. cynomolgi*[15] (**Supplementary Table 6**), in contrast to the one *dbp* and three *dbp* genes identified in *P. vivax* and *P. knowlesi*, respectively. This raises an intriguing hypothesis that *P. vivax* lost one *dbp* gene, and thus its infectivity of Old World monkey erythrocytes, after divergence from a common *P. vivax–P. cynomolgi* ancestor. This hypothesis is also supported by our identification of single-copy *dbp* genes in two other closely related Old World monkey malaria-causing parasites, *Plasmodium fieldi* and *Plasmodium simiovale*, which are incapable of infecting humans[16]. These two Old World monkey species lost one or more *dbp* genes during divergence that confer infectivity to humans, whereas *P. cynomolgi* and *P. knowlesi* retained *dbp* genes that allow invasion of human erythrocytes (**Supplementary Fig. 2**).

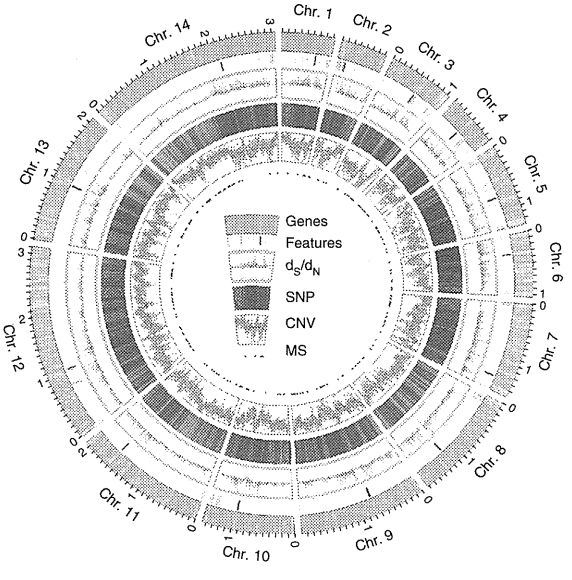

Figure 1 Architecture of the *P. cynomolgi* genome and associated genome-wide variation data. Data are shown for each of the 14 *P. cynomolgi* chromosomes. The six concentric rings, from outermost to innermost, represent (i) the location of 5,049 *P. cynomolgi* genes, excluding those on small contigs (cyan lines); (ii) genome features, including 14 centromeres (thick black lines), 43 telomeric sequence repeats (short red lines), 43 tRNA genes (red lines), 10 rRNAs (dark blue lines) and several gene family members, including 53 *cyir* (dark green lines), 8 *rbp* (brown lines), 13 *sera* (serine-rich antigen; pink lines), 25 *trag* (tryptophan-rich antigen; purple lines), 12 *msp3* (merozoite surface protein 3; light gray lines), 13 *msp7* (merozoite surface protein 7; gray lines), 25 *rad* (silver lines), 8 *etramp* (orange lines), 16 *Pf-fam-b* (light blue lines) and 7 *Pv-fam-d* (light green lines); (iii) plot of d_S/d_N for 4,605 orthologs depicting genome-wide polymorphism within *P. cynomolgi* strains B and Berok (black line) and divergence between *P. cynomolgi* strains B and Berok and *P. vivax* Salvador I (red line); a track above the plot indicates *P. cynomolgi* genes under positive selection (red) and purifying selection (blue), and a track below the plot indicates *P. cynomolgi–P. vivax* orthologs under positive selection (red) and purifying selection (blue); (iv) heatmap indicating SNP density of 3 *P. cynomolgi* strains plotted per 10-kb windows: red, 0–83 SNPs per 10 kb (regions of lowest SNP density); blue, 84–166 SNPs per 10 kb; green, 167–250 SNPs per 10 kb; purple, 251–333 SNPs per 10 kb; orange, 334–416 SNPs per10 kb; yellow, 417–500 SNPs per10 kb (regions of highest SNP density); (v) $\log_2$ ratio plot of CNVs identified from a comparison of *P. cynomolgi* strains B and Berok; and (vi) map of 182 polymorphic intergenic microsatellites (MS, black dots). The figure was generated using Circos software (see URLs).

Table 1 Comparison of genome features between *P. cynomolgi*, *P. vivax* and *P. knowlesi*, three species of the monkey malaria clade

Feature	*P. cynomolgi*	*P. vivax*[12]	*P. knowlesi*[9]
Assembly			
Size (Mb)	26.2	26.9	23.7
Number of scaffolds[a]	14 (1,649)	14 (2,547)	14 (67)
Coverage (fold)	161	10	8
GC content (%)	40.4	42.3	38.8
Genes			
Number of genes	5,722	5,432	5,197
Mean gene length (bp)	2,240	2,164	2,180
Gene density (bp per gene)[b]	4,428.2	4,950.5	4,416.1
Percentage coding[b]	51.0	47.1	49.0
Structural RNAs			
Number of tRNA genes	43	44	41
Number of 5S rRNA genes	3	3	0[c]
Number of 5.8S, 18S and 28S rRNA units	7	7	5
Nuclear genome			
Number of chromosomes	14	14	14
Number of centromeres	14	14	14
Isochore structure[d]	+	+	–
Mitochondrial genome			
Size (bp)[e]	5,986 (AB444123)	5,990 (AY598140)	5,958 (AB444108)
GC content (%)	30.3	30.5	30.5
Apicoplast genome			
Size (bp)	29,297[f]	5,064[g]	N/A
GC content (%)	13.0	17.1	N/A

N/A, not available.
[a]Small unassigned contigs indicated in parentheses. [b]Sequence gaps excluded. [c]Not present in *P. knowlesi* assembly version 4.0. [d]Regions of the genome that differ in density and are separable by CsCl centrifugation; isochores correspond to domains differing in GC content. [e]Identified in other studies (GenBank accessions given in parentheses). [f]Partial sequence (~86% complete) generated during this project. [g]Partial sequence of reference genome only published[12]; actual size is ~35 kb.

We found multiple *rbp* genes, some truncated or present as pseudogenes, in the *P. cynomolgi* genome (**Fig. 1** and **Table 2**). Phylogenetic analysis showed that *rbl* genes from *P. cynomolgi*, *P. vivax* and *P. knowlesi* can be classified into three distinct groups, RBP/NBP-1, RBP/NBP-2 and RBP/NBP-3 (**Supplementary Fig. 3**), and suggests that these groups existed before the three species diverged. All three groups of RBP/NBP are represented in *P. cynomolgi*, whereas *P. vivax* and *P. knowlesi* lack functional genes from the RBP/NBP-3 and RBP/NBP-1 groups, respectively. Thus, *rbl* gene family expansion seems to have occurred after speciation, indicating that the three species have multiple species-specific erythrocyte invasion mechanisms. Notably, we found an ortholog of *P. vivax rbp1b* in some strains of *P. cynomolgi* but not in others (**Supplementary Table 6**). To our knowledge, this is the first example of a CNV for a *rbp* gene between strains of a single *Plasmodium* species, highlighting how repeated creation and destruction of *rbl* genes, a signature of adaptive evolution, may have enabled species of the monkey malaria clade to expand or switch between monkey and human hosts.

The largest gene family in *P. cynomolgi*, consisting of 256 *cyir* (cynomolgi-interspersed repeat) genes, is part of the *pir* (plasmodium-interspersed repeat) superfamily that includes *P. vivax vir* genes ($n = 319$) and *P. knowlesi kir* genes ($n = 70$) (**Table 2**). *Pir*-encoded proteins reside on the surface of infected erythrocytes and have an important role in immune evasion[17]. Most *cyir* genes have sequence similarity to *P. vivax vir* genes ($n = 254$; **Supplementary Table 7**) and are found in subtelomeric regions (**Fig. 1**), but, notably, 11 *cyir* genes have sequence similarity to *P. knowlesi kir* genes (**Supplementary Table 7**) and occur more internally in the chromosomes, as do the *kir* genes in *P. knowlesi*. As with 'molecular mimicry' in *P. knowlesi* (mimicry of host sequences by pathogen sequences)[9], one CYIR protein (encoded by PCYB_032250) has a region of 56 amino acids that is highly similar to the extracellular domain of primate CD99 (**Supplementary Fig. 4**), a molecule involved in the regulation of T-cell function. A new finding is that *P. cynomolgi* has two genes whose sequences are similar to *P. knowlesi SICAvar* genes (**Supplementary Table 7**) that are expressed on the surfaces of schizont-infected macaque erythrocytes and are involved in antigenic variation[18].

The ability to form a dormant hypnozoite stage is common to both *P. cynomolgi* and *P. vivax* and was first shown in laboratory infections of monkeys by mosquito-transmitted *P. cynomolgi*[19]. In a search for candidate genes involved in the hypnozoite stage, we identified nine coding for 'dormancy-related' proteins that had the upstream ApiAP2 motifs[20] necessary for stage-specific transcriptional regulation at the sporozoite (pre-hypnozoite) stage (**Supplementary Table 8**). The candidates include kinases that are involved in cell cycle transition; hypnozoite formation may be regulated by phosphorylation of proteins specifically expressed at the pre-hypnozoite stage. Our list of *P. cynomolgi* candidate genes represents an informed starting point for experimental studies of this elusive stage.

We sequenced *P. cynomolgi* strains Berok (from Malaysia) and Cambodian (from Cambodia) to 26× and 17× coverage, respectively, to characterize *P. cynomolgi* genome-wide diversity through analysis of SNPs, CNVs and microsatellites. A comparison of the three *P. cynomolgi* strains identified 178,732 SNPs (**Supplementary Table 9**) at a frequency of 1 SNP per 151 bp, a polymorphism level somewhat

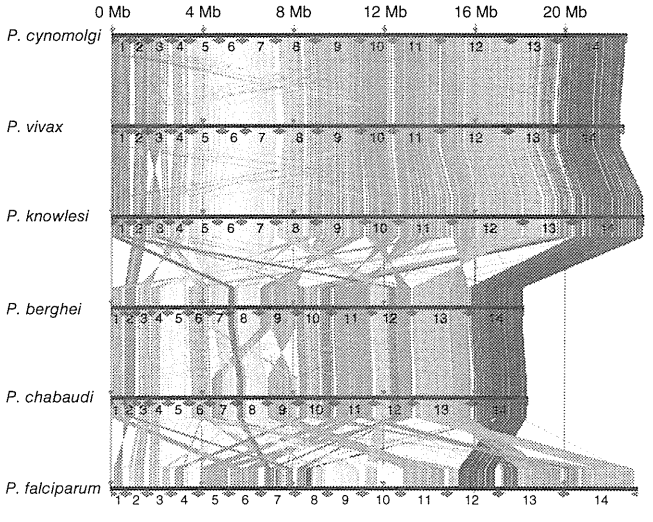

Figure 2 Genome synteny between six species of *Plasmodium* parasite. Protein-coding genes of *P. cynomolgi* are shown aligned with those of five other *Plasmodium* genomes: two species belonging to the monkey malaria clade, *P. vivax* and *P. knowlesi*; two species of rodent malaria, *P. berghei* and *P. chabaudi*; and *P. falciparum*. Highly conserved protein-coding regions between the genomes are colored in order from red (5′ end of chromosome 1) to blue (3′ end of chromosome 14) with respect to genomic position of *P. cynomolgi*.

Table 2 Components of multigene families of *P. cynomolgi*, *P. vivax* and *P. knowlesi* differ in copy number

Family	Multigene family	Localization	Arrangement	*P. cynomolgi*	*P. vivax*	*P. knowlesi*	Putative function and other information
1	*pir* (*vir*-like)	Subtelomeric	Scattered and clustered	254	319[a]	4	Immune evasion
2	*pir* (*kir*-like)	Subtelomeric and central	Scattered and clustered	11	2	66[a]	Immune evasion
3	*SICAvar*	Subtelomeric and central	Scattered and clustered	2	1	242[a]	Antigenic variation, immune evasion
4	*msp3*	Central	Clustered	12	12	3	Merozoite surface protein
5	*msp7*	Central	Clustered	13	13	5	Merozoite surface protein
6	*dbl* (*dbp/ebl*)	Subtelomeric	Scattered	2	1	3	Host cell recognition
7	*rbl* (*rbp/nbp/rh*)	Subtelomeric	Scattered	8[a]	10[a]	3[a]	Host cell recognition
8	*Pv-fam-a* (*trag*)	Subtelomeric	Scattered and clustered	36	36	26[a]	Tryptophan-rich
9	*Pv-fam-b*	Central	Clustered	3	6	1	Unknown
10	*Pv-fam-c*	Subtelomeric	Unknown[b]	1	7	0	Unknown
11	*Pv-fam-d* (*hypb*)	Subtelomeric	Scattered	18	16	2	Unknown
12	*Pv-fam-e* (*rad*)	Subtelomeric	Clustered	27	44	16	Unknown
13	*Pv-fam-g*	Central	Clustered	3	3	3	Unknown
14	*Pv-fam-h* (*hyp16*)	Central	Clustered	6	4	2	Unknown
15	*Pv-fam-i* (*hyp11*)	Subtelomeric	Scattered	6	6	5	Unknown
16	*Pk-fam-a*	Central	Scattered	0	0	12[a]	Unknown
17	*Pk-fam-b*	Subtelomeric	Scattered	0	0	9	Unknown
18	*Pk-fam-c*	Subtelomeric	Scattered	0	0	6[a]	Unknown
19	*Pk-fam-d*	Central	Scattered	0	0	3[a]	Unknown
20	*Pk-fam-e*	Subtelomeric	Scattered	0	0	3[a]	Unknown
21	*PST-A*	Subtelomeric and central	Scattered	9[a]	11[a]	7	αβ hydrolase
22	*ETRAMP*	Subtelomeric	Scattered	9	9	9	Parasitophorous vacuole membrane
23	*CLAG* (*RhopH-1*)	Subtelomeric	Scattered	2	3	2	High-molecular-wieght rhoptry antigen complex
24	*PvSTP1*	Subtelomeric	Unknown[b]	3	10[a]	0	Unknown
25	*PHIST* (Pf-*fam-b*)	Subtelomeric	Scattered and clustered	21	20	15	Unknown
26	*SERA*	Central	Clustered	13[a]	13[a]	8[a]	Cysteine protease

[a]Pseudogenes, truncated genes and gene fragments included. [b]Gene arrangement could not be determined due to localization on unassigned contigs.

similar to that found when *P. falciparum* genomes are compared[21,22]. We calculated the pairwise nucleotide diversity (π) as 5.41×10^{-3} across the genome, which varies little between the chromosomes. We assessed genome-wide CNVs between the *P. cynomolgi* B and Berok strains, using a robust statistical model in the CNV-seq program[23], by which we identified 1,570 CNVs (1 per 17 kb), including 1 containing the *rbp1b* gene on chromosome 7 (**Supplementary Fig. 5**). Finally, mining of the *P. cynomolgi* B and Berok strains identified 182 polymorphic intergenic microsatellites (**Supplementary Table 10**), the first set of genetic markers developed for this species. These provide a toolkit for studies of genetic diversity and population structure of laboratory stocks or natural infections of *P. cynomolgi*, many of which have recently been isolated from screening hundreds of wild monkeys for the zoonosis *P. knowlesi*[24].

We estimated the difference between the number of synonymous changes per synonymous site (d_S) and the number of nonsynonymous changes per nonsynonymous site (d_N) over 4,563 pairs of orthologs within *P. cynomolgi* strains B and Berok and 4,601 pairs of orthologs between these two *P. cynomolgi* strains and *P. vivax* Salvador I, using a simple Nei-Gojobori model[25]. We found 63 genes with $d_N > d_S$ within the two *P. cynomolgi* strains and 3,265 genes with $d_S > d_N$ (**Supplementary Table 11**). Genes with relatively high d_N/d_S ratios include those encoding transmembrane proteins, such as antigens and transporters, among which is a transmission-blocking target antigen, Pcyn230 (encoded by PCYB_042090). Notably, the *P. vivax* ortholog (PVX_003905) does not show evidence for positive selection[26], suggesting species-specific positive selection. We explored the degree to which evolution of orthologs has been constrained between *P. cynomolgi* and *P. vivax* and found 83 genes under possible accelerated evolution but 3,739 genes under possible purifying selection (**Supplementary Table 12**). This conservative estimate indicates that at least 81% of loci have diverged under strong constraint, compared with 1.8% of loci under less constraint or positive selection (**Fig. 1**), indicating that, overall, the genome of *P. cynomolgi* is highly conserved in single-locus genes compared to *P. vivax* and emphasizing the value of *P. cynomolgi* as a biomedical and evolutionary model for studying *P. vivax*.

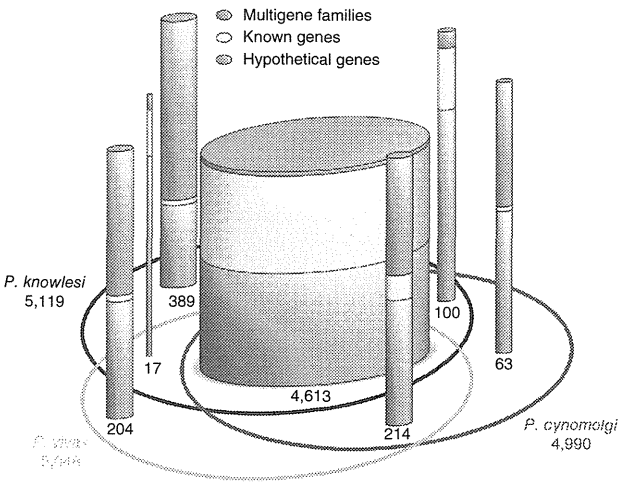

Figure 3 Comparison of the genes of *P. cynomolgi*, *P. vivax* and *P. knowlesi*. The Venn ellipses represent the three genomes, with the total number of genes assigned to the chromosomes indicated under the species name. Cylinders depict orthologous and non-orthologous genes between the three genomes, with the number of genes in each indicated and represented graphically by cylinder relative width. In each cylinder, genes are divided into three categories whose thickness is represented by colored bands proportional to category percentage.

Our generation of the first *P. cynomolgi* genome sequences is a critical step in the development of a robust model system for the intractable and neglected *P. vivax* species[27]. Comparative genome analysis of *P. vivax* and the Old World monkey malaria-causing parasites *P. cynomolgi* and *P. knowlesi* presented here provides the foundation for further insights into traits such as host specificity that will enhance prospects for the eventual elimination of vivax-caused malaria and global malaria eradication.

URLs. PlasmoDB, http://plasmodb.org/; Circos, http://circos.ca/; MIcroSAtelite Identification tool (MISA), http://pgrc.ipk-gatersleben.de/misa/; dbSNP, http://www.ncbi.nlm.nih.gov/projects/SNP/snp_viewBatch.cgi?sbid=1056645.

METHODS

Methods and any associated references are available in the online version of the paper.

Accession codes. Sequence data for the *P. cynomolgi* B, Cambodian and Berok strains have been deposited in the DNA Data Bank of Japan (DDBJ), the European Molecular Biology Laboratory (EMBL) and the GenBank databases under the following accessions: B strain sequence reads DRA000196, genome assembly BAEJ01000001–BAEJ01003341 and annotation DF157093–DF158755; Cambodian strain sequence reads DRA000197; and Berok strain sequence reads SRA047950. SNP calls have been submitted to dbSNP (NYU_CGSB_BIO; 1056645) and may also be downloaded from the dbSNP website (see URLs). Sequences of the *dbp* genes from *P. cynomolgi* (Cambodian strain), *P. fieldi* (A.b.i. strain) and *P. simiovale* (AB617788–AB617791) and the *P. cynomolgi* Berok strain (JQ422035–JQ422036) and *rbp* gene sequences from the *P. cynomolgi* Berok and Cambodian strains (JQ422037–JQ422050) have been deposited. A partial apicoplast genome of the *P. cynomolgi* Berok strain has been deposited (JQ522954). The *P. cynomolgi* B reference genome is also available through PlasmoDB (see URLs).

Note: Supplementary information is available in the online version of the paper.

ACKNOWLEDGMENTS

We thank H. Sawai for suggestions on genome analysis, D. Fisher for help with genome-wide evolutionary analyses and the NYU Langone Medical Center Genome Technology Core for access to Roche 454 sequencing equipment (funded by grant S10 RR026950 to J.M.C. from the US National Institutes of Health (NIH)). Genome and phylogenetic analyses used the Genome Information Research Center in the Research Institute of Microbial Diseases at Osaka University. This work was supported by grants from the Ministry of Education, Culture, Sports, Science and Technology of Japan (18073013, 18GS03140013, 20390120 and 22406012) to K.T., an NIH grant (R01 GM080586) to A.A.E. and a Burroughs Wellcome Fund grant (1007398) and an NIH International Centers of Excellence for Malaria Research grant (U19 AI089676-01) to J.M.C. The content is soley the responsibility of the authors and does not necessarily represent the official views of the NIH.

AUTHOR CONTRIBUTIONS

K.T., J.M.C., A.A.E. and J.W.B. conceived and conducted the study. S.K., Y.K., Y.Y., S.-I.T. and J.W.B. provided *P. cynomolgi* material. S.N., N.G., T.Y. and H.R.K. constructed a computing system for data processing, and S.-I.T., H.H., P.L.S., S.A.S. and H.R.K. performed scaffolding of contigs and manual annotation of the predicted genes. S.N. performed sequence correction of supercontigs and gene prediction. S.-I.T., S.N., N.G., N.A., M.Y., O.K., K.T., H.R.K., R.S., S.A.S. and J.M.C. analyzed data. S.-I.T., N.M.Q.P., T.T., T.M., K.K., J.M.C., T.H., A.A.E., J.W.B. and K.T. wrote the manuscript.

COMPETING FINANCIAL INTERESTS

The authors declare no competing financial interests.

Published online at http://www.nature.com/doifinder/10.1038/ng.2375.
Reprints and permissions information is available online at http://www.nature.com/reprints/index.html.

1. Mendis, K., Sina, B.J., Marchesini, P. & Carter, R. The neglected burden of *Plasmodium vivax* malaria. *Am. J. Trop. Med. Hyg.* **64**, 97–106 (2001).
2. Mueller, I. *et al.* Key gaps in the knowledge of *Plasmodium vivax*, a neglected human malaria parasite. *Lancet Infect. Dis.* **9**, 555–566 (2009).
3. Baird, J.K. Resistance to chloroquine unhinges vivax malaria therapeutics. *Antimicrob. Agents Chemother.* **55**, 1827–1830 (2011).
4. Rayner, J.C., Liu, W., Peeters, M., Sharp, P.M. & Hahn, B.H. A plethora of *Plasmodium* species in wild apes: a source of human infection? *Trends Parasitol.* **27**, 222–229 (2011).
5. Cornejo, O.E. & Escalante, A.A. The origin and age of *Plasmodium vivax*. *Trends Parasitol.* **22**, 558–563 (2006).
6. Escalante, A.A. *et al.* A monkey's tale: the origin of *Plasmodium vivax* as a human malaria parasite. *Proc. Natl. Acad. Sci. USA* **102**, 1980–1985 (2005).
7. Mu, J. *et al.* Host switch leads to emergence of *Plasmodium vivax* malaria in humans. *Mol. Biol. Evol.* **22**, 1686–1693 (2005).
8. Singh, B. *et al.* A large focus of naturally acquired *Plasmodium knowlesi* infections in human beings. *Lancet* **363**, 1017–1024 (2004).
9. Pain, A. *et al.* The genome of the simian and human malaria parasite *Plasmodium knowlesi*. *Nature* **455**, 799–803 (2008).
10. Eyles, D.E., Coatney, G.R. & Getz, M.E. Vivax-type malaria parasite of macaques transmissible to man. *Science* **131**, 1812–1813 (1960).
11. Gibbs, R.A. *et al.* Evolutionary and biomedical insights from the rhesus macaque genome. *Science* **316**, 222–234 (2007).
12. Carlton, J.M. *et al.* Comparative genomics of the neglected human malaria parasite *Plasmodium vivax*. *Nature* **455**, 757–763 (2008).
13. Saxena, A.K., Wu, Y. & Garboczi, D.N. *Plasmodium* p25 and p28 surface proteins: potential transmission-blocking vaccines. *Eukaryot. Cell* **6**, 1260–1265 (2007).
14. Iyer, J., Gruner, A.C., Renia, L., Snounou, G. & Preiser, P.R. Invasion of host cells by malaria parasites: a tale of two protein families. *Mol. Microbiol.* **65**, 231–249 (2007).
15. Okenu, D.M., Malhotra, P., Lalitha, P.V., Chitnis, C.E. & Chauhan, V.S. Cloning and sequence analysis of a gene encoding an erythrocyte binding protein from *Plasmodium cynomolgi*. *Mol. Biochem. Parasitol.* **89**, 301–306 (1997).
16. Coatney, G.R., Collins, W.E., Warren, M. & Contacos, P.G. *The Primate Malarias* (US Department of Health, Education and Welfare, Washington, DC, 1971).
17. Cunningham, D., Lawton, J., Jarra, W., Preiser, P. & Langhorne, J. The *pir* multigene family of *Plasmodium*: antigenic variation and beyond. *Mol. Biochem. Parasitol.* **170**, 65–73 (2010).
18. al-Khedery, B., Barnwell, J.W. & Galinski, M.R. Antigenic variation in malaria: a 3′ genomic alteration associated with the expression of a *P. knowlesi* variant antigen. *Mol. Cell* **3**, 131–141 (1999).
19. Krotoski, W.A. The hypnozoite and malarial relapse. *Prog. Clin. Parasitol.* **1**, 1–19 (1989).
20. Campbell, T.L., De Silva, E.K., Olszewski, K.L., Elemento, O. & Llinas, M. Identification and genome-wide prediction of DNA binding specificities for the ApiAP2 family of regulators from the malaria parasite. *PLoS Pathog.* **6**, e1001165 (2010).
21. Mu, J. *et al.* Genome-wide variation and identification of vaccine targets in the *Plasmodium falciparum* genome. *Nat. Genet.* **39**, 126–130 (2007).
22. Volkman, S.K. *et al.* A genome-wide map of diversity in *Plasmodium falciparum*. *Nat. Genet.* **39**, 113–119 (2007).
23. Xie, C. & Tammi, M.T. CNV-seq, a new method to detect copy number variation using high-throughput sequencing. *BMC Bioinformatics* **10**, 80 (2009).
24. Lee, K.S. *et al.* *Plasmodium knowlesi*: reservoir hosts and tracking the emergence in humans and macaques. *PLoS Pathog.* **7**, e1002015 (2011).
25. Nei, M. & Gojobori, T. Simple methods for estimating the numbers of synonymous and nonsynonymous nucleotide substitutions. *Mol. Biol. Evol.* **3**, 418–426 (1986).
26. Doi, M. *et al.* Worldwide sequence conservation of transmission-blocking vaccine candidate Pvs230 in *Plasmodium vivax*. *Vaccine* **29**, 4308–4315 (2011).
27. Carlton, J.M., Sina, B.J. & Adams, J.H. Why is *Plasmodium vivax* a neglected tropical disease? *PLoS Negl. Trop. Dis.* **5**, e1160 (2011).

ONLINE METHODS

Parasite material. Details of the origin of the *P. cynomolgi* B, Berok and Cambodian strains, their growth in macaques and isolation of parasite material are given in the **Supplementary Note.**

Genome sequencing and assembly. *P. cynomolgi* B strain was sequenced using the Roche 454 GS FLX (Titanium) and Illumina/Solexa Genome Analyzer IIx platforms to 161× coverage. In addition, 2,784 clones (6.8 Mb) of a ~40-kb insert fosmid library in pCC1FOS (EpiCentre Biotechnologies) was sequenced by the Sanger method. A draft assembly of strain B was constructed using a combination of automated assembly and manual gap closure. We first generated *de novo* contigs by assembling Roche 454 reads using GS *De novo* Assembler version 2.0 with default parameters. Contigs of >500 bp were mapped to the *P. vivax* Salvador I reference assembly[12] (PlasmoDB; see URLs). *P. cynomolgi* contigs were iteratively arrayed through alignment to *P. vivax*–assembled sequences with manual corrections. A total of 1,264 aligned contigs were validated by mapping paired-end reads from fosmid clones using blastn ($e < 1 \times 10^{-15}$; identity > 90%; coverage > 200 bp) implemented in GenomeMatcher software version 1.65 (ref. 28). Additional linkages (699 regions) were made using PCR across the intervening sequence gaps with primers designed from neighboring contigs. The length of sequence gaps was estimated from insert lengths of the fosmid paired-end reads, the size of PCR products and homologous sequences of the *P. vivax* genome. Supercontigs were then manually constructed from the aligned contigs. Eventually, we obtained 14 supercontigs corresponding to the 14 chromosomes of the parasite, with a total length of ~22.73 Mb, encompassing ~80% of the predicted *P. cynomolgi* genome. A total of 1,651 contigs (>1 kb) with a total length of 3.45 Mb was identified as unassigned subtelomeric sequences by searching against the *P. vivax* genome using blastn. Additionally, to improve sequence accuracy, we constructed a mapping assembly of Illumina paired-end reads and the 14 supercontigs and unassigned contigs as reference sequences using CLC Genomics Workbench version 3.0 with default settings (CLC Bio). Comparison of the draft *P. cynomolgi* B sequence with 23 *P. cynomolgi* protein-coding genes (64 kb) obtained by Sanger sequencing showed 99.8% sequence identity (**Supplementary Table 13**). The *P. cynomolgi* Berok and Cambodian strains were sequenced to 26× and 17× coverage, respectively, using the Roche 454 GS FLX platform, with single-end and 3-kb paired-end libraries made for the former and a single-end library only made for the latter. For phylogenetic analyses of specific genes, sequences were independently verified by Sanger sequencing (**Supplementary Table 14** and **Supplementary Note**).

Prediction and annotation of genes. Gene prediction for the 14 supercontigs and 1,651 unassigned contigs was performed using the MAKER genome annotation pipeline[29] with *ab initio* gene prediction programs trained on proteins and ESTs from PlasmoDB Build 7.1. For gene annotation, blastn ($e < 1 \times 10^{-15}$; identity > 70%; coverage > 100 bp) searches of *P. vivax* (PvivaxAnnotated Transcripts_PlasmoDB-7.1.fasta) and *P. knowlesi* (PknowlesiAnnotatedTranscripts_PlasmoDB-7.1.fasta) predicted proteomes were run, and the best hits were identified. All predicted genes were manually inspected at least twice for gene structure and functional annotation, and orthologous relationships between *P. cynomolgi*, *P. vivax* and *P. knowlesi* were determined on synteny. A unique identifier, PCYB_######, was assigned to *P. cynomolgi* genes, where the first two of the six numbers indicate chromosome number. Paralogs of genes that seemed to be specific to either *P. cynomolgi*, *P. vivax* or *P. knowlesi* were searched using blastp with default parameters, using a cutoff *e* value of 1×10^{-16}.

Multiple genome sequence alignment. Predicted proteins of *P. cynomolgi* B strain were concatenated and aligned with those from the 14 chromosomes of 5 other *Plasmodium* genomes: *P. vivax*, *P. knowlesi*, *P. falciparum*, *P. berghei* and *P. chabaudi*, using Murasaki software version 1.68.6 (ref. 30).

Search for sequence showing high similarity to host proteins. Eleven *P. cynomolgi* CYIR proteins (with sequence similarity to *P. knowlesi* KIR) were subjected to blastp search for regions having high similarity to host *Macacca mulatta* CD99 protein, with cutoff *e* value of 1×10^{-12} and compositional adjustment (no adjustment) against the nonredundant protein sequence data set of the *M. mulatta* proteome in NCBI.

Phylogenetic analyses. Genes were aligned using ClustalW version 2.0.10 (ref. 31) with manual corrections, and unambiguously aligned sites were selected for phylogenetic analyses. Maximum-likelihood phylogenetic trees were constructed using PROML programs in PHYLIP version 3.69 (ref. 32) under the Jones-Taylor-Thornton (JTT) amino-acid substitution model. To take the evolutionary rate heterogeneity across sites into consideration, the R (hidden Markov model rates) option was set for discrete γ distribution, with eight categories for approximating the site-rate distribution. CODEML programs in PAML 4.4 (ref. 33) were used for estimating the γ shape parameter, α values. For bootstrap analyses, SEQBOOT and CONSENSE programs in PHYLIP were applied.

Candidate genes for hypnozoite formation. We undertook two approaches. First, genes unique to *P. vivax* and *P. cynomolgi* (hypnozoite-forming parasites) and not found in other non-hypnozoite–forming *Plasmodium* species were identified. We used the 147 unique genes identified in the *P. vivax* genome[12] to search the *P. cynomolgi* B sequence. For the orthologs identified in both species, ~1 kb of sequence 5′ to the coding sequence was searched for four specific ApiAP2 motifs[20]—PF14 0633, GCATGC; PF13_0235_D1, GCCCCG; PFF0670w_D1, TAAGCC; and PFD0985w_D2, TGTTAC—which are involved in sporozoite stage–specific regulation and expression (corresponding to the pre-hypnozoite stage). Second, dormancy-related proteins were retrieved from GenBank and used to search for *P. vivax* homologs. Candidate genes ($n = 128$) and orthologs of *P. cynomolgi* and five other parasite species were searched in the region ~1 kb upstream of the coding sequence for the presence of the four ApiAP2 motifs. Data for *P. vivax*, *P. knowlesi*, *P. falciparum*, *P. berghei*, *Plasmodium chabaudi* and *Plasmodium yoelii* were retrieved from PlasmoDB Build 7.1.

Genome-wide screen for polymorphisms. For SNP identification, alignment of Roche 454 data from strains B, Berok and Cambodian was performed using SSAHA2 (ref. 34), with 0.1 mismatch rate and only unique matches reported. Potential duplicate reads generated during PCR amplification were removed, so that when multiple reads mapped at identical coordinates, only the reads with the highest mapping quality were retained. We used a statistical method[35] implemented in SAMtools version 0.1.18 to call SNPs simultaneously in the case of duplicate runs of the same strain. SNPs with high read depth (>100) were filtered out, as were SNPs in poor alignment regions at the ends of chromosomes (**Supplementary Note**).

Nucleotide diversity (π) was calculated as follows. For each site being compared, we calculated allele frequency by counting the two alleles and measured the proportion of nucleotide differences. Letting π be the genetic distance between allele *i* and allele *j*, then the nucleotide diversity within the population is

$$\pi = \sum_{i,j} P_i P_j \pi_{ij}$$

where P_i and P_j are the overall allele frequencies of *i* and *j*, respectively. Mean π was calculated by averaging over sites, weighting each by $\sum_{i=1}^{n-1} \frac{1}{i}$, where *n* is the number of aligned sites. Average d_N/d_S ratios were estimated using the modified Nei-Gojobori/Jukes-Cantor method in MEGA 4 (ref. 36).

CNV-seq[23] was used to identify potential CNVs in *P. cynomolgi*. Briefly, this method is based on a statistical model that allows confidence assessment of observed copy-number ratios from next-generation sequencing data. Roche 454 sequences from *P. cynomolgi* strain B assembly were used as the reference genome, and the *P. cynomolgi* Berok strain was used as a test genome; the sequence coverage of the Cambodian strain was considered too low for analysis. The test reads were mapped to the reference genome, and CNVs were detected by computing the number of reads for each test strain in a sliding window. The validity of the observed ratios was assessed by the computation of a probability of a random occurrence, given no copy-number variation.

Polymorphic microsatellites (defined as repeat units of 1–6 nucleotides) between *P. cynomolgi* strains B and Berok were identified by aligning contigs

from a *de novo* assembly of Berok (generated using Roche GS Assembler version 2.6, with 40-bp minimum overlap, 90% identity) to the B strain using the Burrows-Wheeler Aligner (BWA)[37] and allowing for gaps. Using the Phred-scaled probability of the base being misaligned by SAMtools[35], indel candidates were called from the alignment. In-house Python scripts were used to then cross-reference with the microsatellites found in the reference strain B assembly identified by MISA (see URLs). All homopolymer microsatellites were discarded to account for potential sequence errors introduced by 454 sequencing.

Selective constraint analysis of 4,563 orthologs between *P. cynomolgi* strains B and Berok and 4,601 orthologs between these strains and *P. vivax* Salvador I used MUSCLE[38] alignments with stringent removal of gaps and missing data (*P. cynomolgi* Berok orthologs were identified through a reciprocal best-hit BLAST search against strain B genes). Analyses were conducted using the Nei-Gojobori model[25]. To detect values that could not be explained by chance, we estimated the standard error by a bootstrap procedure with 200 pseudoreplicates for each gene. The expected value for d_S/d_N is 0 if a given pair of sequences is diverging without obvious effects on fitness. In the case of the comparison within *P. cynomolgi*, values with a difference of ± 2 s.e.m. from 0 were considered indicative of an excess of synonymous ($d_S/d_N > 0$) or nonsynonymous ($d_S/d_N < 0$) changes. In the case of the comparison between *P. cynomolgi* and *P. vivax*, we used a more stringent criterion of ± 3 s.e.m. from 0.

28. Ohtsubo, Y., Ikeda-Ohtsubo, W., Nagata, Y. & Tsuda, M. GenomeMatcher: a graphical user interface for DNA sequence comparison. *BMC Bioinformatics* **9**, 376 (2008).
29. Cantarel, B.L. *et al.* MAKER: an easy-to-use annotation pipeline designed for emerging model organism genomes. *Genome Res.* **18**, 188–196 (2008).
30. Popendorf, K., Tsuyoshi, H., Osana, Y. & Sakakibara, Y. Murasaki: a fast, parallelizable algorithm to find anchors from multiple genomes. *PLoS ONE* **5**, e12651 (2010).
31. Thompson, J.D., Higgins, D.G. & Gibson, T.J. CLUSTAL W: improving the sensitivity of progressive multiple sequence alignment through sequence weighting, position-specific gap penalties and weight matrix choice. *Nucleic Acids Res.* **22**, 4673–4680 (1994).
32. Felsenstein, J. *PHYLIP, Phylogeny Inference Package*, 3.6a3 edn (University of Washington, Seattle, 2005).
33. Yang, Z. PAML 4: phylogenetic analysis by maximum likelihood. *Mol. Biol. Evol.* **24**, 1586–1591 (2007).
34. Ning, Z., Cox, A.J. & Mullikin, J.C. SSAHA: a fast search method for large DNA databases. *Genome Res.* **11**, 1725–1729 (2001).
35. Li, H. A statistical framework for SNP calling, mutation discovery, association mapping and population genetical parameter estimation from sequencing data. *Bioinformatics* **27**, 2987–2993 (2011).
36. Tamura, K., Dudley, J., Nei, M. & Kumar, S. MEGA4: Molecular Evolutionary Genetics Analysis (MEGA) software version 4.0. *Mol. Biol. Evol.* **24**, 1596–1599 (2007).
37. Li, H. & Durbin, R. Fast and accurate short read alignment with Burrows-Wheeler transform. *Bioinformatics* **25**, 1754–1760 (2009).
38. Edgar, R.C. MUSCLE: multiple sequence alignment with high accuracy and high throughput. *Nucleic Acids Res.* **32**, 1792–1797 (2004).

Arch Virol
DOI 10.1007/s00705-013-1618-6

ORIGINAL ARTICLE

Dynamics of cellular immune responses in the acute phase of dengue virus infection

Tomoyuki Yoshida · Tsutomu Omatsu · Akatsuki Saito · Yuko Katakai · Yuki Iwasaki · Terue Kurosawa · Masataka Hamano · Atsunori Higashino · Shinichiro Nakamura · Tomohiko Takasaki · Yasuhiro Yasutomi · Ichiro Kurane · Hirofumi Akari

Received: 13 June 2012 / Accepted: 12 December 2012

Abstract In this study, we examined the dynamics of cellular immune responses in the acute phase of dengue virus (DENV) infection in a marmoset model. Here, we found that DENV infection in marmosets greatly induced responses of CD4/CD8 central memory T and NKT cells. Interestingly, the strength of the immune response was greater in animals infected with a dengue fever strain than in those infected with a dengue hemorrhagic fever strain of DENV. In contrast, when animals were re-challenged with the same DENV strain used for primary infection, the neutralizing antibody induced appeared to play a critical role in sterilizing inhibition against viral replication, resulting in strong but delayed responses of CD4/CD8 central memory T and NKT cells. The results in this study may help to better understand the dynamics of cellular and humoral immune responses in the control of DENV infection.

T. Yoshida and T. Omatsu contributed equally to this study.

Electronic supplementary material The online version of this article (doi:10.1007/s00705-013-1618-6) contains supplementary material, which is available to authorized users.

T. Yoshida · Y. Iwasaki · T. Kurosawa · M. Hamano · Y. Yasutomi · H. Akari
Tsukuba Primate Research Center, National Institute of Biomedical Innovation, 1-1 Hachimandai, Tsukuba, Ibaraki 305-0843, Japan

T. Yoshida (✉) · A. Saito · A. Higashino · H. Akari (✉)
Center for Human Evolution Modeling Research, Primate Research Institute, Kyoto University, Inuyama, Aichi 484-8506, Japan
e-mail: yoshida.tomoyuki.4w@kyoto-u.ac.jp

H. Akari
e-mail: akari.hirofumi.5z@kyoto-u.ac.jp

Introduction

Dengue virus (DENV) causes the most prevalent arthropod-borne viral infections in the world [29]. Infection with one of the four serotypes of DENV can lead to dengue fever (DF) and sometimes to fatal dengue hemorrhagic fever (DHF) or dengue shock syndrome (DSS) [12]. The serious diseases are more likely to develop after secondary infection with a serotype of DENV that is different from that of the primary infection. Infection with DENV induces a high-titered neutralizing antibody response that can provide long-term immunity to the homologous DENV serotype, while the effect of the antibody on the heterologous serotypes is transient [22]. On the other hand, enhanced pathogenicity after secondary DENV infection appears to be explained by antibody-dependent enhancement (ADE). Mouse and monkey experiments have shown that subneutralizing levels of DENV-specific antibodies actually enhance infection [1, 6, 11]. Thus, the development of an effective tetravalent dengue vaccine is considered to be an important public-health priority. Recently, several DENV vaccine candidates have undergone clinical trials, and most of them target the induction of neutralizing antibodies [20].

T. Omatsu · T. Takasaki · I. Kurane
Department of Virology I, National Institute of Infectious Diseases, 1-23-1 Toyama, Shinjuku-ku, Tokyo 162-8640, Japan

Y. Katakai
Corporation for Production and Research of Laboratory Primates, 1-1 Hachimandai, Tsukuba, Ibaraki 305-0843, Japan

S. Nakamura
Research Center for Animal Life Science, Shiga University of Medical Science, Seta Tsukinowa-cho, Otsu, Shiga 520-2192, Japan

Published online: 05 February 2013

Research of the long-term immune response in humans has provided several interesting parallels to the data. It was reported that complete cross-protective immunity from heterologous challenge was induced in individuals 1–2 months after a primary DENV infection, with partial immunity present up to 9 months, resulting in a milder disease of shorter duration on reinfection, and that complete serotype-specific immunity against symptomatic dengue was observed up to 18 months postinfection [30]. Guzman and Sierra have previously recorded the long-term presence of both DENV-specific antibodies and T cells up to 20 years after natural infections [10, 31]. Of note, increased T cell activation is reportedly associated with severe dengue disease [7, 8]. Thus, the balance between humoral and cellular immunity may be important in the control of dengue diseases.

However, the details regarding the implication of humoral and cellular immunity in controlling DENV infection remain to be elucidated. Previously, passive transfer of either monoclonal or polyclonal antibodies was shown to protect against homologous DENV challenge [13, 15, 16]. It was also reported that neutralizing antibodies played a greater role than cytotoxic T lymphocyte (CTL) responses in heterologous protection against secondary DENV infection *in vivo* in IFN-$\alpha/\beta R^{-/-}$ and IFN$\gamma R^{-/-}$ mouse models [18]. Moreover, $CD4^+$ T cell depletion did not affect the DENV-specific IgG or IgM Ab titers or their neutralizing activity in the IFN$\gamma R^{-/-}$ mouse model [36]. On the other hand, there are several reports showing that cellular immunity rather than humoral immunity plays an important role in the clearance of DENV. For example, in adoptive transfer experiments, although cross-reactive DENV-1-specific $CD8^+$ T cells did not mediate protection against a lethal DENV-2 infection, adoptive transfer of $CD4^+$ T cells alone mediated protection and delayed mortality in IFN-$\alpha/\beta R^{-/-}$ and IFN$\gamma R^{-/-}$ mouse models [39]. It has also been demonstrated that $CD8^+$ T lymphocytes have a direct role in protection against DENV challenge in the IFN-$\alpha/\beta R^{-/-}$ mouse model of DENV infection by depleting $CD8^+$ T cells [35]. In addition, previous data from adoptive-transfer experiments in BALB/c mice showed that cross-reactive memory $CD8^+$ T cells were preferentially activated by the secondary DENV infection, resulting in augmented IFN-γ and tumor necrosis factor-α (TNF-α) responses, and this effect was serotype-dependent [2, 3]. Although it has previously been suggested that inducing neutralizing antibodies against DENV may play an important role in controlling DENV infection, CTLs are also proposed to contribute to clearance during primary DENV infection and to pathogenesis during secondary heterologous infection in the BALB/c mouse model [4].

Why did the mouse models of DENV infection show inconsistent results *in vivo*? One of the reasons could be that these results were obtained mainly from genetically manipulated mice such as IFN-$\alpha/\beta R^{-/-}$ and IFN$\gamma R^{-/-}$ mice. Moreover, these mice were inoculated with 10^9–10^{10} genome equivalents (GE) of DENV [27, 35, 36], which were likely in large excess compared with the 10^4-10^5 GE of DENV injected into humans by a mosquito [19]. In addition, the efficiency of DENV replication in wild mice *in vivo* is very low compared to that in humans [35].

Recently, novel non-human primate models of DENV infection using rhesus macaques as well as marmosets and tamarins have been developed [24–26, 38]. An intravenous challenge of rhesus macaques with a high dose of virus inoculum (1×10^7 GE) of DENV-2 resulted in readily visible hemorrhaging, which is one of the cardinal symptoms of human DHF [26]. It was also shown that the cellular immune response was activated due to expression of IFN-γ, TNF-α, and macrophage inflammatory protein-1 β in $CD4^+$ and $CD8^+$ T cells during primary DENV infection in rhesus macaques [20]. On the other hand, in the marmoset model of DENV infection, we observed high levels of viremia (10^5–10^7 GE/ml) after subcutaneous inoculation with 10^4–10^5 plaque-forming units (PFU) of DENV-2. Moreover, we demonstrated that DENV-specific IgM and IgG were consistently detected and that the DENV-2 genome was not detected in any of these marmosets inoculated with the same DENV-2 strain used in the primary infection [24]. It is notable that while neutralizing antibody titers were at levels of 1:20-1:80 before the re-challenge inoculation, the titers increased up to 1:160-1:640 after the re-challenge inoculation [24]. These results suggested that the secondary infection with DENV-2 induced a protective humoral immunity to DENV-2 and that DENV-infected marmoset models may be useful in order to analyze the relationship between DENV replication and the dynamics of adaptive immune responses *in vivo*.

Taking these findings into consideration, we investigated the dynamics of cellular immunity in response to primary and secondary DENV infection in the marmoset model.

Materials and methods

Animals

All animal studies were conducted in accordance with protocols of experimental procedures that were approved by the Animal Welfare and Animal Care Committee of the National Institute of Infectious Diseases, Japan, and the National Institute of Biomedical Innovation, Japan. A total of six male marmosets, weighing 258–512 g, were used. Common marmosets were purchased from Clea Japan Inc.

(Tokyo, Japan) and caged singly at 27 ± 2 °C in 50 ± 10 % humidity with a 12-h light-dark cycle (lighting from 7:00 to 19:00) at Tsukuba Primate Research Center, National Institute of Biomedical Innovation, Tsukuba, Japan. Animals were fed twice a day with a standard marmoset diet (CMS-1M, CLEA Japan) supplemented with fruit, eggs and milk. Water was given ad libitum. The animals were in healthy condition and confirmed to be negative for anti-dengue-virus antibodies before inoculation with dengue virus [24].

Cells

Cell culture was performed as described previously [24]. Vero cells were cultured in minimum essential medium (MEM, Sigma) with 10 % heat-inactivated fetal bovine serum (FBS, GIBCO) and 1 % non-essential amino acid (NEAA, Sigma) at 37 °C in 5 % CO_2. C6/36 cells were cultured in MEM with 10 % FBS and 1 % NEAA at 28 °C in 5 % CO_2.

Virus

DENV type 2 (DENV-2) strain DHF0663 (accession no. AB189122) and strain D2/Hu/Maldives/77/2008NIID (Mal/77/08) were used for inoculation studies. The DENV-2, DHF0663 strain was isolated from a DHF case in Indonesia. The DENV-2 Mal/77/08 strain was isolated from imported DF cases from the Maldives. For all DENV strains, isolated clinical samples were propagated in C6/36 cells and were used within four passages on C6/36 cells. Culture supernatant from infected C6/36 cells was

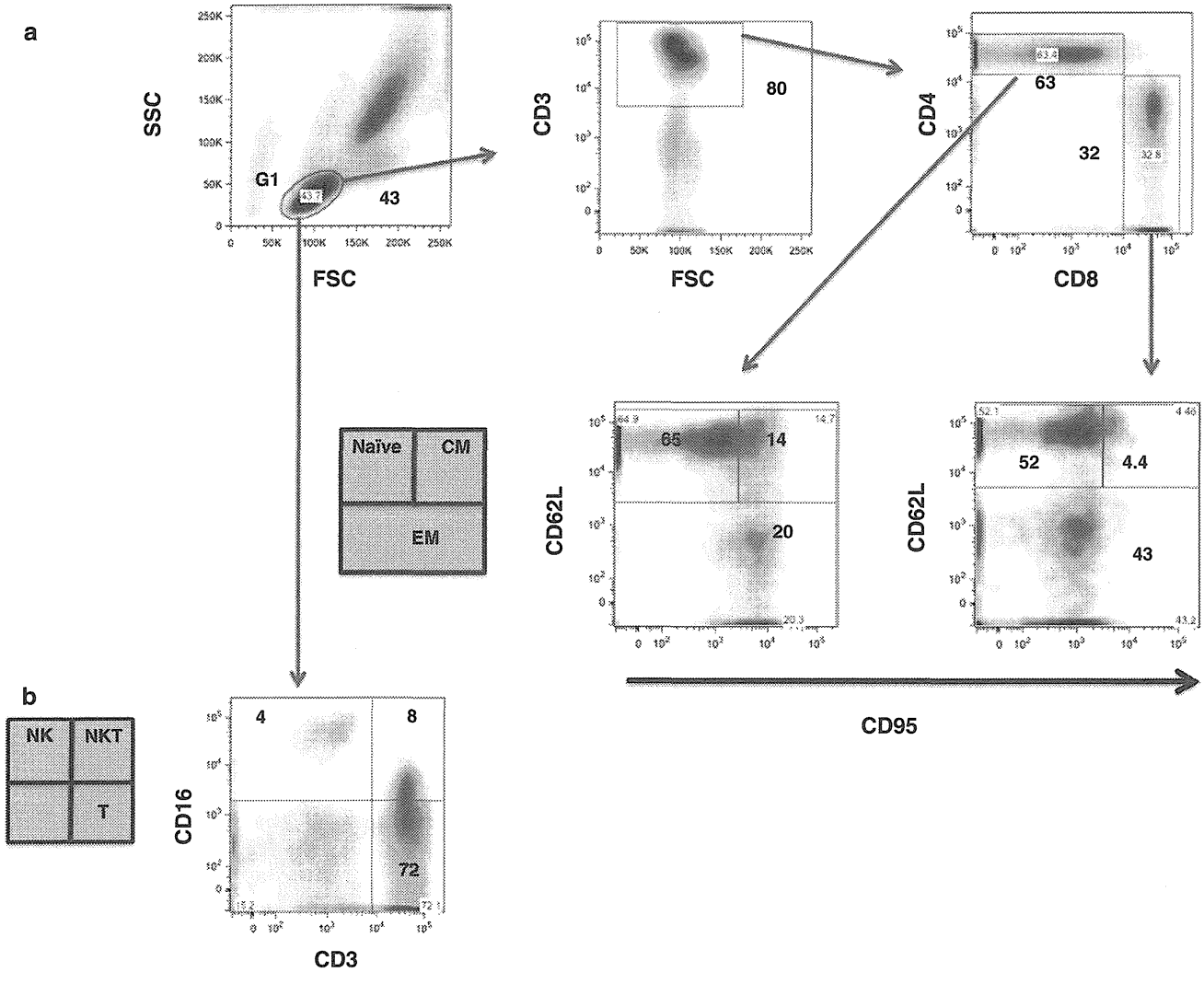

Fig. 1 Flow cytometric analysis of naïve, central/effector memory T cells and NK/NKT cells in marmosets. (**a**) Gating strategy to indentify CD4 and CD8 T, NK and NKT cells. The G1 population was selected and analyzed for CD4 and CD8 T, NK and NKT cells. (**a**) Profiling of naïve, central memory, and effector memory CD4 and CD8 T cells in total CD4 and CD8 T cells. (**b**) Profiling of NK and NKT cells in total lymphocytes. Results shown are representative of three healthy marmosets used in this study

centrifuged at 3,000 rpm for 5 min to remove cell debris and then stored at −80 °C until use.

Infection of the marmosets with DENV

In the challenge experiments, profiling of the key adaptive and innate immune cells in the marmosets after infection with DENV-2 was done. For primary DENV infection, four marmosets were inoculated subcutaneously in the back with either 1.9×10^5 PFU of the DENV-2 Mal/77/08 strain (Cj08-007, Cj07-011) or 1.8×10^4 PFU of the DHF0663 strain (Cj07-006, Cj07-008) [24]. In the case of the DENV re-challenge experiment, two marmosets initially inoculated with 1.8×10^5 PFU of the DHF0663 strain were re-inoculated 33 weeks after the primary challenge with 1.8×10^5 PFU of the same strain (Cj07-007, Cj07-014) [24]. Blood samples were collected on days 0, 1, 3, 7, 14, and 21 after inoculation and were used for virus titration and flow cytometric analysis. Inoculation with DENV and blood drawing were performed under anesthesia with 5 mg/kg of ketamine hydrochloride. Day 0 was defined as the day of virus inoculation. The viral loads in marmosets obtained in a previous study are shown in Supplementary Figure 1 [24].

Flow cytometry

Flow cytometry was performed as described previously [37]. Fifty microliters of whole blood from marmosets was stained with combinations of fluorescence-conjugated monoclonal antibodies; anti-CD3 (SP34-2; Becton Dickinson), anti-CD4 (L200; BD Pharmingen), anti-CD8 (CLB-T8/4H8; Sanquin), anti-CD16 (3G8; BD Pharmingen), anti-CD95 (DX2; BD Pharmingen), and anti-CD62L (145/15; Miltenyi Biotec). Then, erythrocytes were lysed with FACS lysing solution (Becton Dickinson). After washing with a sample buffer containing phosphate-buffered saline (PBS) and 1 % FBS, the labeled cells were resuspended in a fix buffer containing PBS and 1 % formaldehyde. The expression of these markers on the lymphocytes was analyzed using a FACSCanto II flow cytometer (Becton Dickinson). The data analysis was conducted using FlowJo software (Treestar, Inc.). Results are shown as mean ± standard deviation (SD) for the marmosets used in this study.

Table 1 Subpopulation ratios of lymphocytes in marmosets

Subpopulation name	Subpopulation ratios (Mean ± SD: %)
$CD3^+$	75.7 ± 6.4
$CD3^+CD4^+$	65.4 ± 6.8
$CD3^+CD4^+CD62L^+CD95^-$ (CD4 T_N)	65.9 ± 3.7
$CD3^+CD4^+CD62L^+CD95^+$(CD4 T_{CM})	16.4 ± 2.9
$CD3^+CD4^+CD62LCD95^{\pm}$ (CD4 T_{EM})	19.5 ± 2.5
$CD3^+CD8^+$	29.0 ± 8.0
$CD3^+CD8^+CD62L^+CD95^-$ (CD8 T_N)	66.7 ± 10.2
$CD3^+CD8^+CD62L^+CD95^+$(CD8 T_{CM})	4.7 ± 3.6
$CD3^+CD8^+CD62LCD95^{\pm}$ (CD8 T_{EM})	28.8 ± 14.8
CD3CD16 + (NK)	4.2 ± 2.6
$CD3^+CD16^+$ (NKT)	5.1 ± 3.4

SD: Standard deviation

Results shown are mean ± SD from 3 healthy marmosets

Results

Naïve central/effector memory T cells and NK/NKT cells in marmosets

Basic information regarding CD4/CD8 naïve and central/effector memory T cells and NK/NKT cells in common marmosets was unavailable. Thus, we examined the immunophenotypes of lymphocyte subsets in the marmosets (Fig. 1). The gating strategy for profiling the CD4 and CD8 T cells in the marmosets by FACS is shown in Fig. 1a. Human T cells are classically divided into three functional subsets based on their cell-surface expression of CD62L and CD95, i.e., $CD62L^+CD95^-$ naive T cells (T_N), $CD62L^+CD95^+$ central memory T cells (T_{CM}), and $CD62L^-CD95^{\pm}$ effector memory T cells (T_{EM}) [9, 21, 28]. In this study, $CD4^+$ and $CD8^+$ T_N, T_{CM}, and T_{EM} subpopulations were defined as $CD62L^+CD95^-$, $CD62L^+CD95^+$, and $CD62L^-CD95^{\pm}$, respectively (Fig. 1a and Table 1). The average ratio of $CD3^+$ T lymphocytes in the total lymphocytes of three marmosets was found to be 75.7 ± 6.4 %. The average ratio of $CD4^+$ T cells in the $CD3^+$ subset was 65.4 ± 6.8 %. The average ratios of $CD4^+$ T_N, T_{CM}, and T_{EM} cells were 65.9 ± 3.7 %, 16.4 ± 2.9 %, 19.5 ± 2.5 %, respectively. The average ratio of $CD8^+$ T cells in the $CD3^+$ subset was 29.0 ± 8.0 %. The average ratios of $CD8^+$ T_N, T_{CM}, and T_{EM} cells were 66.7 ± 10.2 %, 4.7 ± 3.6 %, 28.8 ± 14.8 %, respectively.

We recently characterized a $CD16^+$ major NK cell subset in tamarins and compared NK activity in tamarins with or without DENV infection [37, 38]. In terms of NKT cells, NK1.1 (CD161) and CD1d are generally used as markers of NKT cells [32]. However, these anti-human NK1.1 and CD1d antibodies are unlikely to cross-react with the NKT cells of the marmosets. Thus, we defined NKT cells as a population expressing both CD3 and CD16 as reported previously [14, 17]. The NK and NKT cell subsets were determined to be $CD3^-CD16^+$ and $CD3^+CD16^+$ lymphocytes in the marmosets. The average ratios of NK and NKT cell subsets in the lymphocytes were 4.2 ± 2.6 % and 5.1 ± 3.4 %, respectively (Table 1). We observed that the proportions of the major lymphocyte

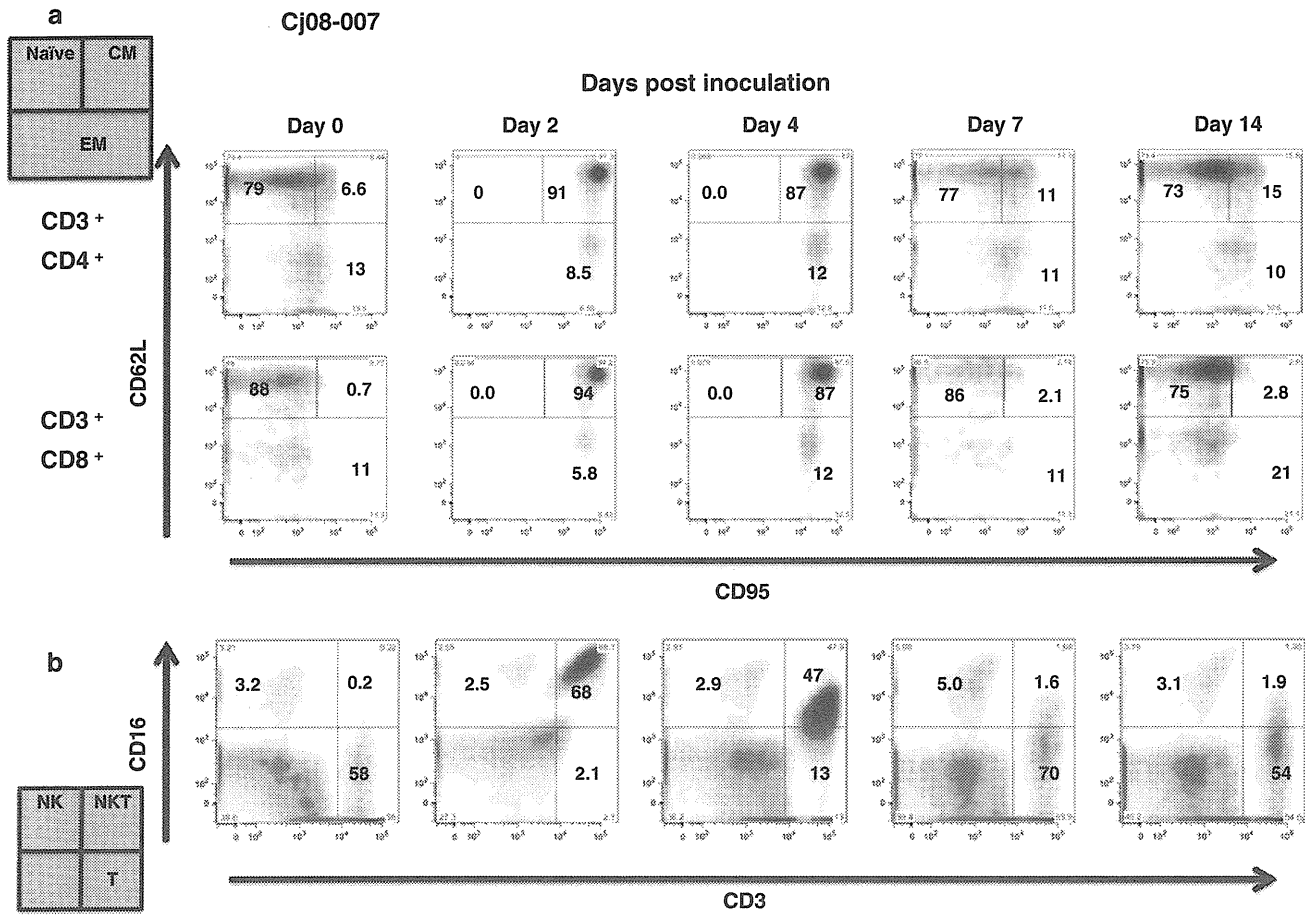

Fig. 2 Profiling of CD4 and CD8 T, NK and NKT cells in marmosets with primary infection with the DENV-2 Mal/77/08 strain. For primary DENV infection, two marmosets were inoculated subcutaneously in the back with 1.9×10^5 PFU of the DENV-2 Mal/77/08 strain. (**a**) Profiling of naïve, central memory, and effector memory CD4 and CD8 T cells in total CD4 and CD8 T cells. (**b**) Profiling of NK and NKT cells in total lymphocytes. (**a-b**) Cj08-007

subsets in the marmosets were similar to those in cynomolgus monkeys and tamarins [37, 38].

Profiling of CD4 and CD8 T, NK and NKT cells in marmosets after primary infection with DENV-2 (Mal/77/08 strain)

We investigated the cellular immune responses against DENV-2 DF strain (Mal/77/08) in marmosets. Dengue vRNA was detected in plasma samples from two marmosets on day 2 postinfection (Supplementary Fig. 1a). For the two marmosets (Cj08-007, Cj07-011), the plasma levels of vRNA reached their peaks at 9.6×10^6 and 7.0×10^6 GE/ml, respectively, on day 4 postinfection. Plasma vRNA was detected in both marmosets on days 2, 4, and 7. We then examined the profiles and frequencies of the CD4 and CD8 T, NK and NKT cells in the infected marmosets (Figs. 2–3 and Table 2). $CD4^+$ T_{CM} cells drastically increased to 88.7 ± 2.8 % from 13 ± 0.4 % between day 0 and day 2 post-inoculation (Table 2). Reciprocally, $CD4^+$ T_N cells decreased to 1.6 ± 3.3 % from 74.1 ± 0.9 % at the same time. $CD4^+$ T_{EM} cells maintained the initial levels throughout the observation period. $CD8^+$ T_{CM} cells increased to 91.9 ± 5.5 % from 2.1 ± 0.8 % between day 0 day 2 post-inoculation, and reciprocally, $CD8^+$ T_N cells decreased to 2.5 ± 4.7 % from 89.9 ± 2.5 % at the same time. In addition, NK cells maintained their initial levels throughout the observation period. However, NKT cells drastically increased to 52.6 ± 17 % from 0.2 ± 0.0 % between day 0 and day 2 post-inoculation. These results suggest that CD4/CD8 T and NKT cells may efficiently respond to the Mal/77/08 strain of DENV.

Profiling of CD4 and CD8 T, NK and NKT cells in the marmosets after primary infection with DENV-2 (DHF0663 strain)

Next, we investigated cellular immune responses against another DENV-2 DHF strain (DHF0663) in marmosets.

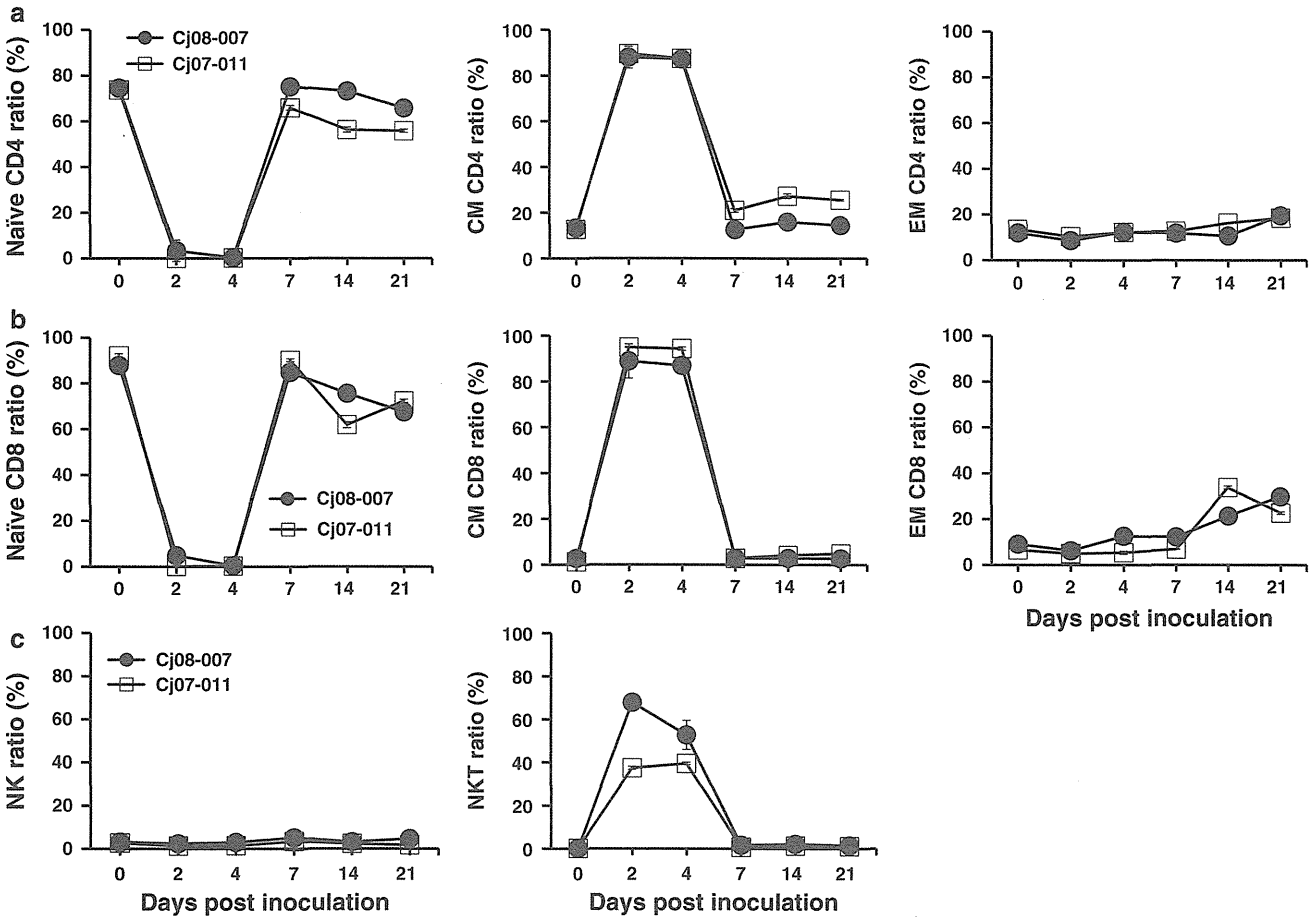

Fig. 3 Frequency of CD4 and CD8 T, NK and NKT cells in marmosets with primary infection with the DENV-2 Mal/77/08 strain. For primary DENV infection, two marmosets were inoculated subcutaneously in the back with 1.9×10^5 PFU of the DENV-2 Mal/77/08 strain. (**a**) Ratios of naïve, central memory, and effector memory CD4 T cells in total CD4 T cells. (**b**) Ratios of naïve, central memory, and effector memory CD8 T cells in total CD8 T cells. (**c**) Ratios of NK and NKT cells in total lymphocytes. (**a-c**) Cj08-007, Cj07-011

Table 2 Subpopulation ratios of lymphocytes in marmosets during primary DENV infection (Mal/77/08)

Subpopulation name		Subpopulation ratio (Mean ± SD: %)					
		Days after inoculation					
		Day 0	Day 2	Day 4	Day 7	Day 14	Day 21
$CD3^+CD4^+CD62L^+CD95''$	($CD4\ T_N$)	74.1 ± 0.9	1.6 ± 3.3	0.2 ± 0.3	70.5 ± 5.5	64.8 ± 9.7	60.8 ± 5.9
$CD3^+CD4^+CD62L^+CD95^+$	($CD4\ T_{CM}$)	13 ± 0.4	88.7 ± 2.8	87.4 ± 0.2	16.8 ± 5.0	21.6 ± 6.5	20 ± 6.4
$CD3^+CD4^+CD62LCD95^±$	($CD4\ T_{EN}$)	12.8 ± 0.9	9.5 ± 1.0	12.3 ± 0.4	12.3 ± 0.5	134 ± 3.2	189 ± 1.4
$CD3^+CD8^+CD62L^+CD95^-$	($CD8\ T_N$)	89.9 ± 2.5	2.5 ± 4.7	0.3 ± 0.3	87.5 ± 3.3	68.7 ± 79	69.8 ± 3.1
$CD3^+CD8^+CD62L^+CD95^+$	($CD8\ T_{CM}$)	2.1 ± 0.8	91.9 ± 5.5	90.6 ± 4.2	2.8 ± 0.5	3.5 ± 08	3.8 ± 1.2
$CD3^+CD8^+CD62LCD95^±$	($CD8\ T_{EN}$)	7.8 ± 1.6	5.6 ± 0.8	9.0 ± 4.1	9.5 ± 3.1	27.6 ± 72	26.3 ± 4.3
$CD3^-CD16+$	(NK)	2.9 ± 0.2	1.8 ± 0.6	2.2 ± 0.9	4.2 ± 0.9	2.8 ± 04	3.2 ± 1.7
$CD3^+CD16^+$	(NKT)	0.2 ± 0.0	52.6 ± 17	46.1 ± 8.5	1.1 ± 05	1.7 ± 05	1.2 ± 0.2

SD: Standard deviation

Results shown are mean ± SD from two marmosets as shown in Figure 3

Dengue vRNA was detected in plasma samples from the marmosets on day 2 post-infection ([24], Supplementary Fig. 1b). For the two marmosets (Cj07-006, Cj07-008), the plasma vRNA levels were found to be 3.4×10^5 and 3.8×10^5 GE/ml on day 2 and 2.0×10^6 and 9.4×10^5 GE/ml, respectively, at the peak on day 4 post-infection and became undetectable by day 14. Thus, we examined the profiles and frequencies of the $CD4^+$ and $CD8^+$ T, NK and NKT cells in these DENV-infected marmosets (Fig. 4–5 and Table 3). It was found that on day 7 post-inoculation, $CD4^+$ and $CD8^+$ T_N cells decreased, and in contrast, the T_{CM} populations increased in both marmosets; however, the changes in proportion were much less pronounced than in the case of the marmosets infected with the DF strain. We observed no consistent tendency in the kinetics of $CD4^+$ and $CD8^+$ T_{EM} cells nor in NK and NKT cells. These results suggest that the strength of T cell responses may be dependent on the strain of DENV.

Profiling of CD4 and CD8 T, NK and NKT cells in marmosets re-challenged with a DENV-2 strain

In order to examine the cellular immune responses against re-challenge with a DENV-2 DHF strain in the marmoset model, marmosets were infected twice with the same DENV-2 strain (DHF0663) with an interval of 33 weeks after the primary infection. The results showed that vRNA and NS1 antigens were not detected in plasma and that the neutralizing antibody titer was obviously increased after the secondary infection. The data indicated that the primary infection induced protective immunity, including a neutralizing antibody response to re-challenge with the same DENV strain ([24]; Supplementary Fig. 1c). We also investigated the profiles of the CD4 and CD8 T, NK and NKT cells in the marmosets (Cj07-007, Cj07-014) that were re-challenged with the same DENV-2 strain (DHF0663) (Figs. 6–7). $CD4^+$ T_{CM} cells drastically increased on day 14 post-inoculation. On the other hand,

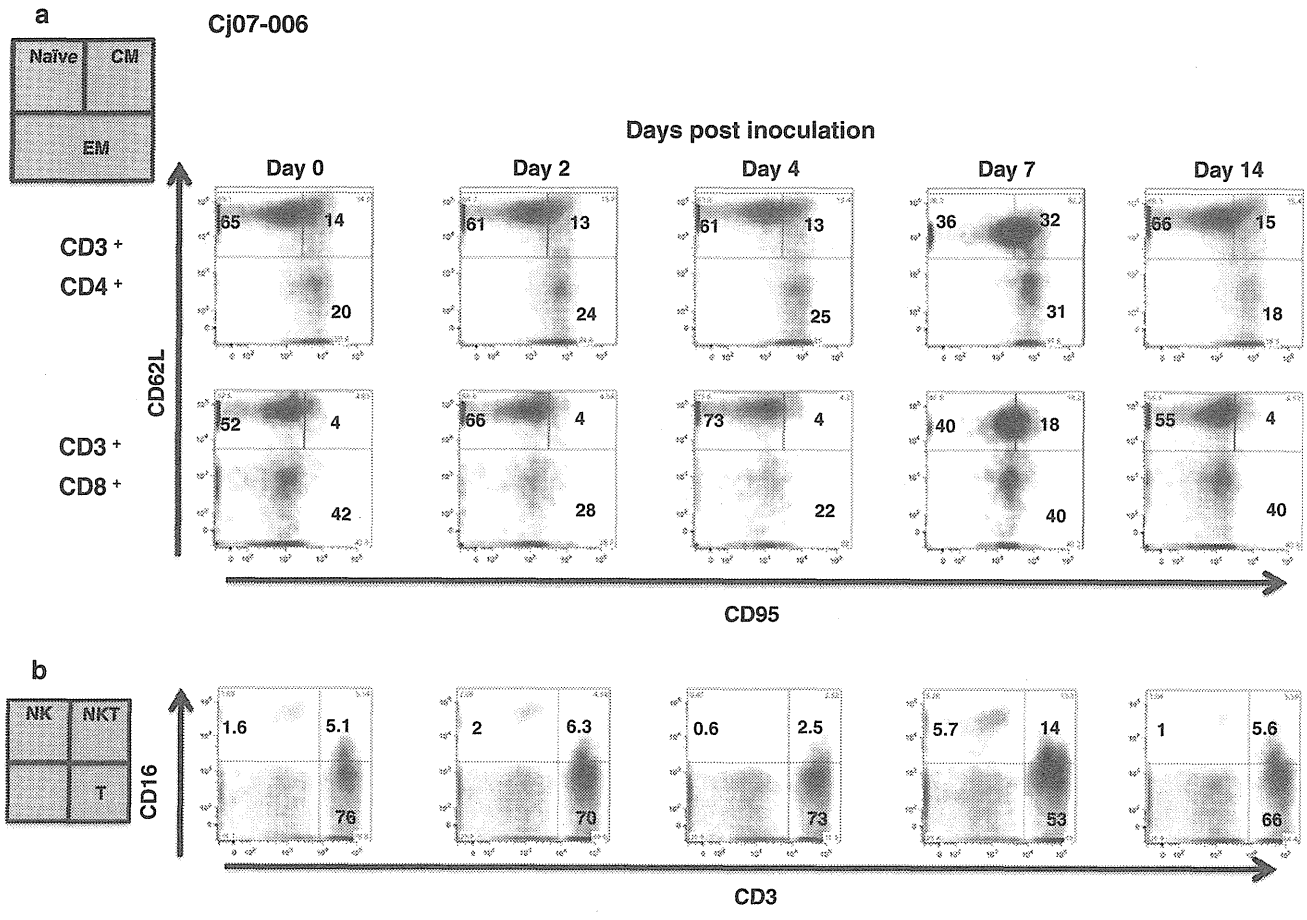

Fig. 4 Profiling of CD4 and CD8 T, NK and NKT cells in marmosets with primary infection with the DENV-2 DHF0663 strain. For primary DENV infection, two marmosets were inoculated subcutaneously in the back with 1.8×10^4 PFU of the DENV-2 DHF0663 strain. (**a**) Profiling of naïve, central memory, and effector memory CD4 and CD8 T cells in total CD4 and CD8 T cells. (**b**) Profiling of NK and NKT cells in total lymphocytes. (**a-b**) Cj07-006

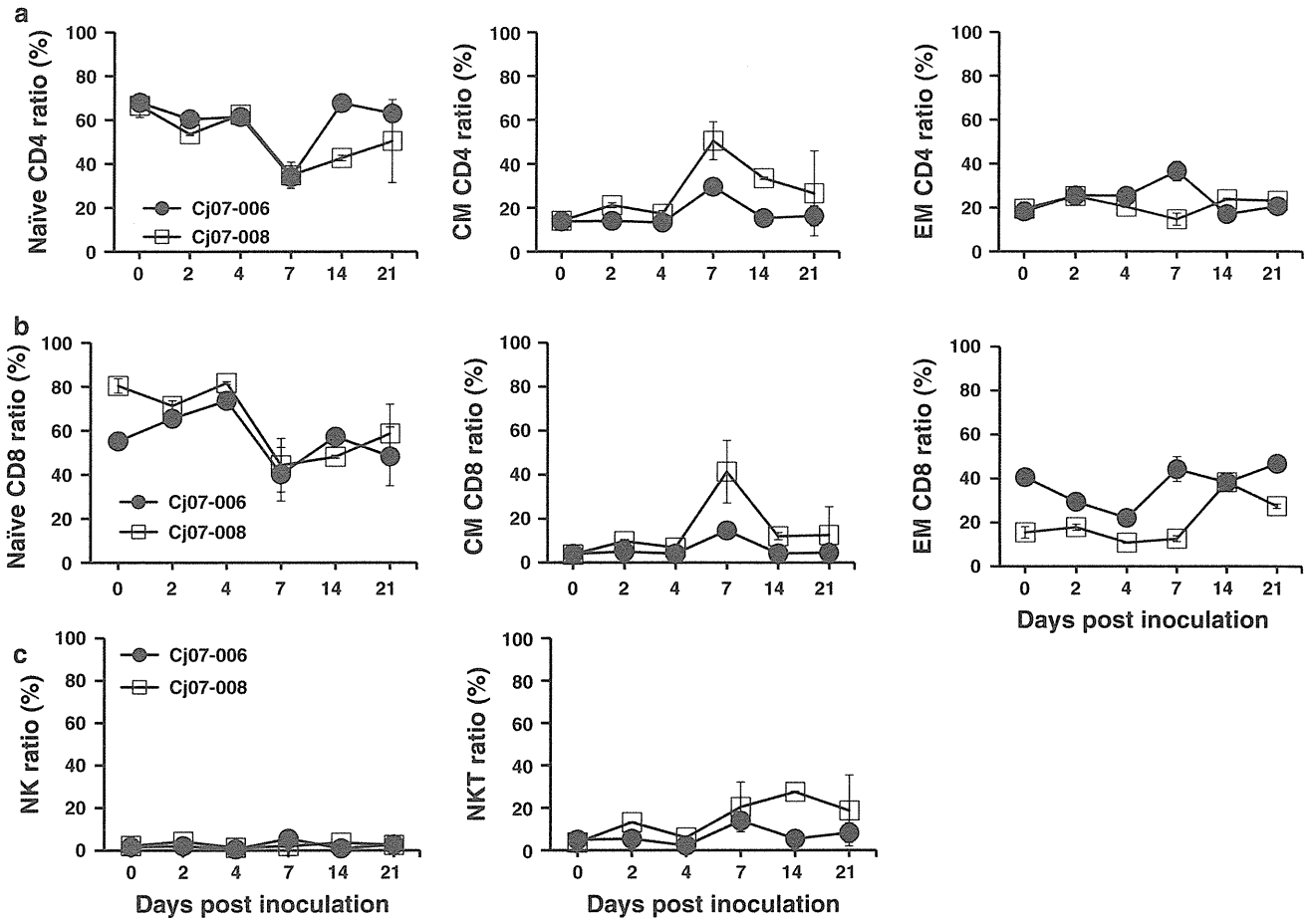

Fig. 5 Frequency of CD4 and CD8 T, NK and NKT cells in marmosets with primary infection with the DENV-2 DHF0663 strain. For primary DENV infection, two marmosets were inoculated subcutaneously in the back with 1.8×10^4 PFU of the DENV-2 DHF0663 strain. (**a**) Ratios of naïve, central memory, and effector memory CD4 T cells in total CD4 T cells. (**b**) Ratios of naïve, central memory, and effector memory CD8 T cells in total CD8 T cells. (**c**) Ratios of NK and NKT cells in total lymphocytes. (**a-c**) Cj07-006, Cj07-008

Table 3 Subpopulation ratios of lymphocytes in marmosets during primary DENV infection (DHF0663)

Subpopulation name		Subpopulation ratios (Mean ± SD: %)					
		Days after inoculation					
		Day 0	Day 2	Day 4	Day 7	Day1 4	Day 21
$CD3^+CD4^+CD62L^+CD95^-$	($CD4\ T_N$)	67.3 ± 3.6	57.0 ± 4.0	61.9 ± 0.9	34.4 ± 3.6	55.2 ± 14	56.7 ± 13
$CD3^+CD4^+CD62L^+CD95^+$	($CD4T_{CM}$)	13.9 ± 1.3	17.5 ± 4.1	15.2 ± 2.5	40.0 ± 13	33.8 ± 10	21.3 ± 12
$CD3^+CD8^+CD62L^-CD95^{\pm}$	($CD4\ T_{EM}$)	18.8 ± 2.2	25.3 ± 0.9	22.8 ± 2.9	25.6 ± 13	20.3 ± 4.0	21.8 ± 1.5
$CD3^+CD8^+CD62L^+CD95^-$	($CDS\ T_N$)	67.8 ± 14	68.4 ± 3.7	77.7 ± 4.6	42.2 ± 7.4	52.7 ± 5.5	53.5 ± 9.8
$CD3^+CD8^+CD62L^+CD95^-$	($CDS\ T_{CM}$)	3.9 ± 0.6	7.4 ± 2.8	5.5 ± 1.6	28 ± 17	8.1 ± 4.6	8.6 ± 8.9
$CD3^+CD8^+CD62L^-CD95^{\pm}$	($CDS\ T_{EM}$)	28 ± 14	23.5 ± 6.7	16.4 ± 6.5	28.3 ± 18	38.2 ± 1.9	37.0 ± 11
$CD3^-CD16^+$	(NK)	4.7 ± 1.0	4.2 ± 1.9	2.0 ± 1.1	6.3 ± 2.3	5.1 ± 2.2	7.3 ± 1.2
$CD3^+CD16^+$	(NKT)	7.8 ± 1.0	9.3 ± 4.5	5.9 ± 2.6	22.6 ± 8.4	20.6 ± 10	17.3 ± 10

SD: Standard deviation

Results shown are mean ± SD from 2 marmosets as shown in Figure 5

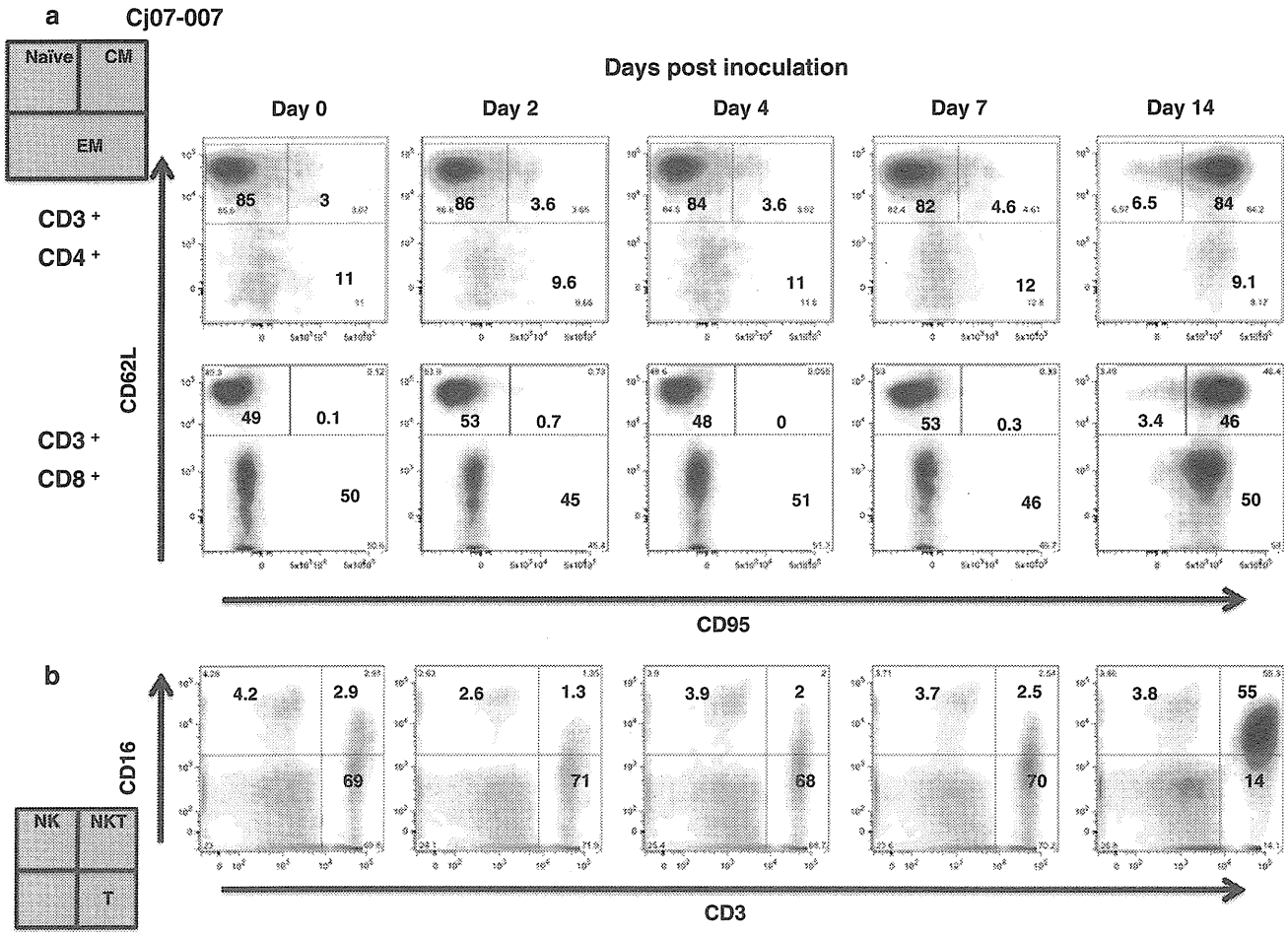

Fig. 6 Profiling of CD4 and CD8 T, NK and NKT cells in marmosets after re-challenge with the DENV-2 DHF0663 strain. Two marmosets that were initially inoculated with 1.8×10^5 PFU of the DHF0663 strain were re-inoculated 33 weeks after the primary challenge with 1.8×10^5 PFU of the same strain. (**a**) Profiling of naïve, central memory, and effector memory CD4 and CD8 T cells in total CD4 and CD8 T cells. (**b**) Profiling of NK and NKT cells in total lymphocytes. (**a**-**b**) Cj07-007

$CD4^+$ T_N cells decreased strongly at the same time. $CD4^+$ T_{EM} cells maintained their initial levels through the observation period. Similarly, $CD8^+$ T_{CM} and NKT cells clearly increased on day 14 post-inoculation. Importantly, these T cell responses were induced one week after the obvious induction of the neutralizing antibody in the marmosets [24]. These results suggest that the neutralizing antibody may play a critical role in the complete inhibition of the secondary DENV infection.

Discussion

In this study, we demonstrated the dynamics of the central/effector memory T cells and NK/NKT subsets against DENV infection in our marmoset model. First, we characterized the central/effector memory T and NK/NKT subsets in marmosets (Fig. 1). Second, we found that CD4/CD8 central memory T cells and NKT cells had significant responses in the primary DENV infection, and the levels appeared to be dependent on the strain of the virus employed for challenge experiments (Figs. 2–5). Finally, we found delayed responses of CD4/CD8 central memory T cells in the monkeys re-challenged with the same DENV DHF strain, despite the complete inhibition of DENV replication (Figs. 6–7).

The present study shed light on the dynamics of cellular and humoral immune responses against DENV *in vivo* in the marmoset model. Our results showed that cellular immune responses were induced earlier than antibody responses in the primary infection. Thus, our results suggest the possibility that cellular immunity may contribute, at least in part, to the control of primary DENV infection. On the other hand, in the presence of neutralizing antibodies in the re-challenged monkeys [24], delayed (on day 14 after the re-challenge) responses of CD4/CD8 central memory T cells were observed despite the complete inhibition of DENV replication. These results indicate that

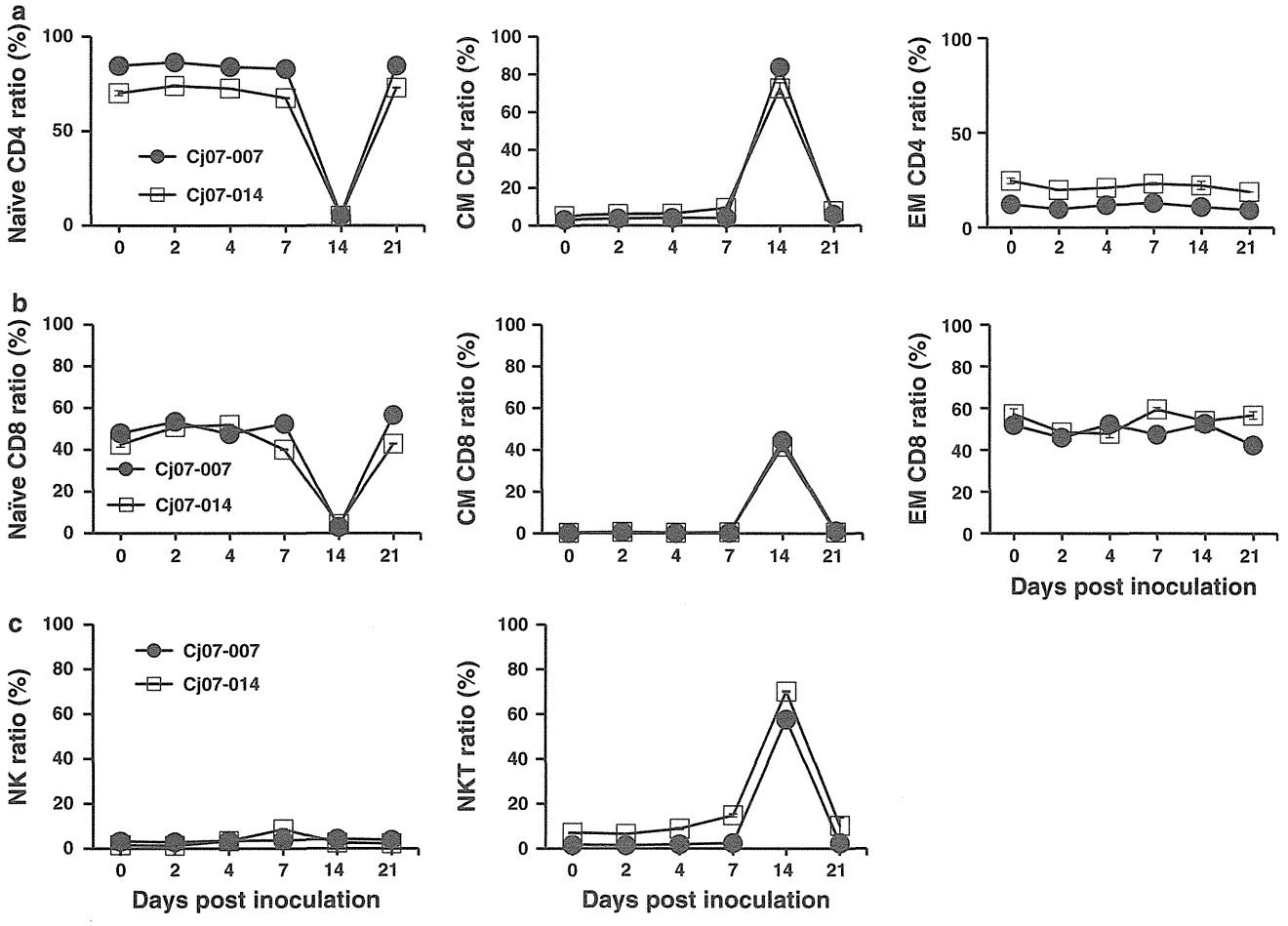

Fig. 7 Frequency of CD4 and CD8 T, NK and NKT cells in marmosets after re-challenge with the DENV-2 DHF0663 strain. Two marmosets initially inoculated with 1.8×10^5 PFU of the DHF0663 strain were re-inoculated 33 weeks after the primary challenge with 1.8×10^5 PFU of the same strain. (**a**) Ratios of naïve, central memory, and effector memory CD4 T cells in total CD4 T cells. (**b**) Ratios of naïve, central memory, and effector memory CD8 T cells in total CD8 T cells. (**c**) Ratios of NK and NKT cells in total lymphocytes. (**a**-**c**) Cj07-007, Cj07-014

cellular immunity is unlikely to play a major role in the control of DENV re-infection. Alternatively, it is still possible that components of cellular immunity, such as memory T cells, could partially play a helper role for the enhanced induction of neutralizing antibodies even without an apparent increase in the proportion of T_{CM}, resulting in efficient prevention of DENV replication.

It is possible that the DENV strains used in this study influence the strength of cellular immune responses. The differences in cellular immune responses between the monkeys infected with the DF and DHF strains are probably not caused by individual differences in the marmosets, because the FACS results were consistent with each pair of marmosets. It was shown previously that there was a reduction in CD3, CD4, and CD8 cells in DHF and that lower levels of CD3, CD4, and CD8 cells discriminated DHF from DF patients during the febrile stage of illness [5]. There was a significant increase in an early activation marker on $CD8^+$ T cells in children with DHF compared with DF during the febrile period of illness [8]. Another group reported that levels of peripheral blood mononuclear cell apoptosis were higher in children developing DHF [23]. Moreover, cDNA array and ELISA screening demonstrated that IFN-inducible genes, IFN-induced genes and IFN production were strongly up-regulated in DF patients when compared to DHF patients, suggesting a significant role of the IFN system during infection with DF strains when compared to DHF strains [34]. Thus, it is reasonable to assume that DHF strains might have the ability to negatively regulate T cell responses. A recent report demonstrating that the sequence of a DHF strain differed from that of a DF strain at six unique amino acid residues located in the membrane, envelope and non-structural genes [33], which supports our notion.

Alternatively, another possibility is that the strength of T cell responses might depend on the viral load. In fact, in

our results, the stronger T cell responses in monkeys infected with the DF strain were paralleled by higher viral loads, which was in contrast to the result obtained with DHF-strain-infected animals with lower viral loads. Of note, the tenfold higher challenge dose of the DF strain used in this study (1.9×10^5 PFU) compared to the DHF strain (1.8×10^4 PFU) could have simply led to tenfold higher peak viral RNA levels in monkeys infected with the DF strain. In either case, the relationship between the strength of the antiviral immune response and the viral strain remains to be elucidated. Further *in vivo* characterization of the antiviral immunity and the viral replication kinetics induced by infection with various DENV strains isolated from DF and DHF patients will help to understand the mechanism of differential disease progression in the course of DENV infection.

We observed that dengue vRNA was not detected in plasma samples from marmosets re-infected with the same DENV-2 DHF strain 33 weeks after the primary infection. This result suggests that memory B cells induced in the primary DENV infection were predominantly activated to produce neutralizing antibodies against the same DHF strain in the secondary infection in the absence of apparent cellular immune responses. A previous report showed that DENV infection induces a high-titered neutralizing antibody that can provide long-term immunity to the homologous DENV serotype [22], which is consistent with our results. By contrast, the role of cellular immune responses in the control of DENV infection remains to be elucidated. Our results in this study may suggest that cellular immune responses and neutralizing antibodies acted cooperatively to control primary DENV infection. In DENV-infected patients, it may be difficult to distinguish whether each case is primary or secondary DENV infection and also to serially collect blood samples for immunological study in the course of the infection, which is likely to be the reason for the discrepancy regarding the importance of cellular immunity in DENV infection. From this point of view, our marmoset model of DENV infection will further provide important information regarding the role of cellular immune responses in DENV infection.

Acknowledgments We would like to give special thanks to members of The Corporation for Production and Research of Laboratory Primates for technical assistance. We also appreciate Ms. Tomoko Ikoma and Mizuho Fujita for technical assistance. This work was supported by grants from the Ministry of Health, Labor and Welfare of Japan, and by the Environment Research and Technology Development Fund (D-1007) from the Ministry of the Environment of Japan.

Conflict of interest The authors declare that the research was conducted in the absence of any commercial or financial relationships that could be construed as a potential conflict of interest.

References

1. Balsitis SJ, Williams KL, Lachica R, Flores D, Kyle JL, Mehlhop E, Johnson S, Diamond MS, Beatty PR, Harris E (2010) Lethal antibody enhancement of dengue disease in mice is prevented by Fc modification. PLoS Pathog 6:e1000790
2. Beaumier CM, Mathew A, Bashyam HS, Rothman AL (2008) Cross-reactive memory CD8(+) T cells alter the immune response to heterologous secondary dengue virus infections in mice in a sequence-specific manner. J Infect Dis 197:608–617
3. Beaumier CM, Rothman AL (2009) Cross-reactive memory CD4+ T cells alter the CD8+ T-cell response to heterologous secondary dengue virus infections in mice in a sequence-specific manner. Viral Immunol 22:215–219
4. Beaumier CM, Jaiswal S, West KY, Friberg H, Mathew A, Rothman AL (2010) Differential in vivo clearance and response to secondary heterologous infections by H2(b)-restricted dengue virus-specific CD8+ T cells. Viral Immunol 23:477–485
5. Fadilah SA, Sahrir S, Raymond AA, Cheong SK, Aziz JA, Sivagengei K (1999) Quantitation of T lymphocyte subsets helps to distinguish dengue hemorrhagic fever from classic dengue fever during the acute febrile stage. Southeast Asian J Trop Med Public Health 30:710–717
6. Goncalvez AP, Engle RE, St Claire M, Purcell RH, Lai CJ (2007) Monoclonal antibody-mediated enhancement of dengue virus infection in vitro and in vivo and strategies for prevention. Proc Natl Acad Sci USA 104:9422–9427
7. Green S, Pichyangkul S, Vaughn DW, Kalayanarooj S, Nimmannitya S, Nisalak A, Kurane I, Rothman AL, Ennis FA (1999) Early CD69 expression on peripheral blood lymphocytes from children with dengue hemorrhagic fever. J Infect Dis 180: 1429–1435
8. Green S, Vaughn DW, Kalayanarooj S, Nimmannitya S, Suntayakorn S, Nisalak A, Lew R, Innis BL, Kurane I, Rothman AL, Ennis FA (1999) Early immune activation in acute dengue illness is related to development of plasma leakage and disease severity. J Infect Dis 179:755–762
9. Gupta S, Gollapudi S (2008) CD95-mediated apoptosis in naive, central and effector memory subsets of CD4+ and CD8+ T cells in aged humans. Exp Gerontol 43:266–274
10. Guzman MG, Alvarez M, Rodriguez-Roche R, Bernardo L, Montes T, Vazquez S, Morier L, Alvarez A, Gould EA, Kouri G, Halstead SB (2007) Neutralizing antibodies after infection with dengue 1 virus. Emerg Infect Dis 13:282–286
11. Halstead SB (1979) In vivo enhancement of dengue virus infection in rhesus monkeys by passively transferred antibody. J Infect Dis 140:527–533
12. Halstead SB (2007) Dengue. Lancet 370:1644–1652
13. Henchal EA, Henchal LS, Schlesinger JJ (1988) Synergistic interactions of anti-NS1 monoclonal antibodies protect passively immunized mice from lethal challenge with dengue 2 virus. J Gen Virol 69(Pt 8):2101–2107
14. Hus I, Staroslawska E, Bojarska-Junak A, Dobrzynska-Rutkowska A, Surdacka A, Wdowiak P, Wasiak M, Kusz M, Twardosz A, Dmoszynska A, Rolinski J (2011) CD3+/CD16+CD56+ cell numbers in peripheral blood are correlated with higher tumor burden in patients with diffuse large B-cell lymphoma. Folia Histochem Cytobiol 49:183–187
15. Kaufman BM, Summers PL, Dubois DR, Eckels KH (1987) Monoclonal antibodies against dengue 2 virus E-glycoprotein protect mice against lethal dengue infection. Am J Trop Med Hyg 36:427–434
16. Kaufman BM, Summers PL, Dubois DR, Cohen WH, Gentry MK, Timchak RL, Burke DS, Eckels KH (1989) Monoclonal

antibodies for dengue virus prM glycoprotein protect mice against lethal dengue infection. Am J Trop Med Hyg 41:576–580
17. Khvedelidze M, Chkhartishvili N, Abashidze L, Dzigua L, Tsertsvadze T (2008) Expansion of CD3/CD16/CD56 positive NKT cells in HIV/AIDS: the pilot study. Georgian Med News 165:78–83
18. Kyle JL, Balsitis SJ, Zhang L, Beatty PR, Harris E (2008) Antibodies play a greater role than immune cells in heterologous protection against secondary dengue virus infection in a mouse model. Virology 380:296–303
19. Mathew A, Rothman AL (2008) Understanding the contribution of cellular immunity to dengue disease pathogenesis. Immunol Rev 225:300–313
20. Mladinich KM, Piaskowski SM, Rudersdorf R, Eernisse CM, Weisgrau KL, Martins MA, Furlott JR, Partidos CD, Brewoo JN, Osorio JE, Wilson NA, Rakasz EG, Watkins DI (2012) Dengue virus-specific CD4+ and CD8+ T lymphocytes target NS1, NS3 and NS5 in infected Indian rhesus macaques. Immunogenetics 64:111–121
21. Mueller YM, Makar V, Bojczuk PM, Witek J, Katsikis PD (2003) IL-15 enhances the function and inhibits CD95/Fas-induced apoptosis of human CD4+ and CD8+ effector-memory T cells. Int Immunol 15:49–58
22. Murphy BR, Whitehead SS (2011) Immune response to dengue virus and prospects for a vaccine. Annu Rev Immunol 29:587–619
23. Myint KS, Endy TP, Mongkolsirichaikul D, Manomuth C, Kalayanarooj S, Vaughn DW, Nisalak A, Green S, Rothman AL, Ennis FA, Libraty DH (2006) Cellular immune activation in children with acute dengue virus infections is modulated by apoptosis. J Infect Dis 194:600–607
24. Omatsu T, Moi ML, Hirayama T, Takasaki T, Nakamura S, Tajima S, Ito M, Yoshida T, Saito A, Katakai Y, Akari H, Kurane I (2011) Common marmoset (Callithrix jacchus) as a primate model of dengue virus infection: development of high levels of viremia and demonstration of protective immunity. J Gen Virol 92:2272–2280
25. Omatsu T, Moi ML, Takasaki T, Nakamura S, Katakai Y, Tajima S, Ito M, Yoshida T, Saito A, Akari H, Kurane I (2013) Changes in hematological and serum biochemical parameters in common marmosets (Cllithrix jacchus) after inoculation with dengue virus. J Med Primatol 54:89–98
26. Onlamoon N, Noisakran S, Hsiao HM, Duncan A, Villinger F, Ansari AA, Perng GC (2010) Dengue virus-induced hemorrhage in a nonhuman primate model. Blood 115:1823–1834
27. Pawitan JA (2011) Dengue virus infection: predictors for severe dengue. Acta Med Indones 43:129–135
28. Pitcher CJ, Hagen SI, Walker JM, Lum R, Mitchell BL, Maino VC, Axthelm MK, Picker LJ (2002) Development and homeostasis of T cell memory in rhesus macaque. J Immunol 168:29–43
29. Rigau-Perez JG, Clark GG, Gubler DJ, Reiter P, Sanders EJ, Vorndam AV (1998) Dengue and dengue haemorrhagic fever. Lancet 352:971–977
30. Sabin AB (1950) The dengue group of viruses and its family relationships. Bacteriol Rev 14:225–232
31. Sierra B, Garcia G, Perez AB, Morier L, Rodriguez R, Alvarez M, Guzman MG (2002) Long-term memory cellular immune response to dengue virus after a natural primary infection. Int J Infect Dis 6:125–128
32. Terabe M, Berzofsky JA (2008) The role of NKT cells in tumor immunity. Adv Cancer Res 101:277–348
33. Tuiskunen A, Monteil V, Plumet S, Boubis L, Wahlstrom M, Duong V, Buchy P, Lundkvist A, Tolou H, Leparc-Goffart I (2011) Phenotypic and genotypic characterization of dengue virus isolates differentiates dengue fever and dengue hemorrhagic fever from dengue shock syndrome. Arch Virol 156:2023–2032
34. Ubol S, Masrinoul P, Chaijaruwanich J, Kalayanarooj S, Charoensirisuthikul T, Kasisith J (2008) Differences in global gene expression in peripheral blood mononuclear cells indicate a significant role of the innate responses in progression of dengue fever but not dengue hemorrhagic fever. J Infect Dis 197:1459–1467
35. Yauch LE, Zellweger RM, Kotturi MF, Qutubuddin A, Sidney J, Peters B, Prestwood TR, Sette A, Shresta S (2009) A protective role for dengue virus-specific CD8+ T cells. J Immunol 182:4865–4873
36. Yauch LE, Prestwood TR, May MM, Morar MM, Zellweger RM, Peters B, Sette A, Shresta S (2010) CD4+ T cells are not required for the induction of dengue virus-specific CD8+ T cell or antibody responses but contribute to protection after vaccination. J Immunol 185:5405–5416
37. Yoshida T, Saito A, Iwasaki Y, Iijima S, Kurosawa T, Katakai Y, Yasutomi Y, Reimann KA, Hayakawa T, Akari H (2010) Characterization of natural killer cells in tamarins: a technical basis for studies of innate immunity. Front Microbiol 1:128
38. Yoshida T, Omatsu T, Saito A, Katakai Y, Iwasaki Y, Iijima S, Kurosawa T, Hamano M, Nakamura S, Takasaki T, Yasutomi Y, Kurane I, Akari H (2012) CD16(+) natural killer cells play a limited role against primary dengue virus infection in tamarins. Arch Virol 157:363–368
39. Zompi S, Santich BH, Beatty PR, Harris E (2012) Protection from secondary dengue virus infection in a mouse model reveals the role of serotype cross-reactive B and T cells. J Immunol 188:404–416

OPEN ACCESS Freely available online

PLOS ONE

A Large Extension to HIV-1 Gag, Like Pol, Has Negative Impacts on Virion Assembly

Hiyori Haraguchi[1], Takeshi Noda[2], Yoshihiro Kawaoka[2,3,4], Yuko Morikawa[1]*

1 Kitasato Institute for Life Sciences, Kitasato University, Minato-ku, Tokyo, Japan, **2** Institute of Medical Science, University of Tokyo, Minato-ku, Tokyo, Japan, **3** ERATO Infection-Induced Host Responses Project, Japan Science and Technology Agency, Saitama, Japan, **4** Influenza Research Institute, Department of Pathological Sciences, University of Wisconsin-Madison, Madison, Wisconsin, United States of America

Abstract

The GagPol protein of HIV-1 harbors viral enzymes, such as protease (PR), reverse transcriptase, and integrase, that are all crucial for virion infectivity. Previous studies have suggested that expression of GagPol alone does not produce viral particles and that the budding defect is caused by the presence of the Pol region. However, it has remained unknown why GagPol fails to produce viral particles. We show here that HIV-1 GagPol is incapable of membrane binding and subsequent particle assembly. Our confocal data indicated that, despite full N-myristoylation, GagPol protein failed to target plasma membrane with diffuse distribution in the cytoplasm. Membrane flotation analysis confirmed these findings. Progressive C-terminal truncation of GagPol to give GagPR allowed for plasma membrane targeting but still not for particle production. Conversely, the C-terminal addition of a noncognate protein, such as ß-galactosidase or 4 tandem GFP, to Gag impaired the membrane affinity, indicating that the Pol region, a large extension to Gag, inhibits membrane binding in the context of GagPol. The addition of the 10 N-terminal amino acids of Fyn kinase [Fyn(10)], a tight membrane-binding signal, conferred plasma membrane targeting on GagPol, but the Fyn(10)GagPol did not produce viral particles. The defect in particle budding was not rescued by the introduction of the PTAP motif, which is responsible for a late stage of viral particle budding. Rather, electron microscopy suggested that the budding defect of GagPR occurred at an early stage of particle morphogenesis. Our data, which were consistent with previous observations, demonstrate the defects of GagPol in membrane binding and particle assembly.

Citation: Haraguchi H, Noda T, Kawaoka Y, Morikawa Y (2012) A Large Extension to HIV-1 Gag, Like Pol, Has Negative Impacts on Virion Assembly. PLoS ONE 7(10): e47828. doi:10.1371/journal.pone.0047828

Editor: David Harrich, Queensland Institute of Medical Research, Australia

Received June 13, 2012; **Accepted** September 17, 2012; **Published** October 23, 2012

Funding: This study was funded by Grant-in-Aid for Scientific Research (B) 22390091 (http://www.jsps.go.jp/index.html), Health Labour Sciences Research grant, Research on HIV/AIDS (http://www.mhlw.go.jp). The funders had no role in study design, data collection and analysis, decision to publish, or preparation of the manuscript.

Competing Interests: The authors have declared that no competing interests exist.

* E-mail: morikawa@lisci.kitasato-u.ac.jp

Introduction

The human immunodeficiency virus type 1 (HIV-1) genome contains three major genes, *gag*, *pol*, and *env*, that encode the viral structural protein Gag, enzymatic polyprotein Pol, and envelope protein Env, respectively. The *gag* gene is translated into a Gag precursor protein that is subsequently cleaved into the p17/matrix (MA), p24/capsid (CA), p7/nucleocapsid (NC), and p6 domains by HIV-1 protease during virion maturation. The *pol* gene is translated into a GagPol precursor protein by −1 ribosomal frameshifting, which occurs at an efficiency of 5–10% during Gag synthesis, resulting in the generation of a 10–20:1 ratio of Gag to GagPol [1,2]. GagPol is essential for viral replication, since the Pol region harbors viral-specific enzymes [protease (PR), reverse transcriptase (RT), and integrase (IN)] that are indispensable for virion infectivity.

The Gag protein is a driving force for retroviral particle assembly. This process consists of several distinct but mutually interdependent steps, including the membrane targeting and multimerization of Gag as well as the pinching off of budded particles from the membrane. In HIV-1, Gag multimerization is driven by the CA to NC domain [3–7]. The membrane-binding domain for HIV-1 Gag is composed of an N-terminal myristoylation signal [8,9] and a cluster of basic residues in MA [10], both of which are required for tight membrane binding of Gag [10]. Nuclear magnetic resonance (NMR) studies have suggested a myristoyl switch model in which the N-myristoyl moiety is exposed upon the binding of phosphatidylinositol 4,5-bisphosphate [PI(4,5)P_2] to the basic residues [11]. Although the N-myristoyl moiety is not directly involved in Gag multimerization, several studies have suggested that myristoyl exposure is regulated by Gag multimerization [12–15]. HIV-1 particle budding requires the sequential recruitment of the host endosomal protein sorting complex required for transport (ESCRT) components to the site of particle assembly [16,17]. Like other retroviruses, the p6 domain contains the late domain (the PTAP motif) that interacts with the ESCRT components [16,18–20]. A number of studies indicate that HIV-1 Gag primarily targets the plasma membrane, where particle assembly and budding occur [21–26], although Gag also can initiate assembly in endosomes and then be transported to the cell surface [27–34].

In contrast, GagPol itself lacks the ability to produce viral particles and incorporates into viral particles only through coassembly with Gag [35–39]. The N-terminal region of GagPol is identical with the major part of Gag (MA-CA-NC). However, GagPol lacks the p6 domain and instead contains the p6* domain,